

Optimal Transmit Antenna Deployment and Power Allocation for Wireless Power Supply in an Indoor Space

KENNETH M. MAYER[Ⓧ] (Graduate Student Member, IEEE),
LAURA COTTATELLUCCI[Ⓧ] (Member, IEEE), AND ROBERT SCHOBER[Ⓧ] (Fellow, IEEE)

¹Institute for Digital Communications, Department of Electrical Engineering, Friedrich-Alexander University Erlangen-Nuremberg, Germany.

CORRESPONDING AUTHOR: Kenneth M. Mayer (e-mail: kenneth.m.mayer@fau.de).

This work was (partly) funded by the Deutsche Forschungsgemeinschaft (DFG, German Research Foundation) – SFB 1483 – Project-ID 442419336, EmpkinS.

ABSTRACT As Internet of Things (IoT) devices proliferate, sustainable methods for powering them are becoming indispensable. The wireless provision of power enables battery-free operation and is crucial for complying with weight and size restrictions. For the energy harvesting (EH) components of these devices to be small, a high operating frequency is necessary. In conjunction with a large transmit antenna, the receivers may be located in the radiating near-field (Fresnel) region, e.g., in indoor scenarios. In this paper, we propose a wireless power transfer (WPT) system ensuring reliable supply of power to an arbitrary number of mobile, low-power, and single-antenna receivers, whose locations in a three-dimensional cuboid room are unknown. A max-min optimisation problem is formulated to determine the optimal transmit power distribution. We rigorously prove that the optimal transmit power distribution's support has a lower dimensionality than its domain and thus, the employment of a continuous aperture antenna, utilised in Holographic MIMO (HMIMO), is unnecessary in the context of the considered WPT problem. Indeed, deploying a discrete transmit antenna architecture, i.e., a transmit antenna array, is sufficient and our proposed solution provides the optimal transmit antenna deployment and power allocation. Moreover, for a one-dimensional transmit antenna architecture, a finite number of transmit antennas is proven to be optimal. The proposed optimal solution is validated through computer simulations. Our simulation results indicate that the optimal transmit antenna architecture requires a finite number of transmit antennas and depends on the geometry of the environment and the dimensionality of the transmit antenna array. The robustness of the solution, which is obtained under the assumption that a line-of-sight (LoS) link exists between the transmitter and receiver, is assessed in an isotropic scattering environment containing a strong LoS component.

INDEX TERMS Wireless power transfer, optimisation, radiating near-field region.

I. INTRODUCTION

THE number of Internet of Things (IoT) devices continues to grow rapidly and is expected to exceed 43 billion devices globally by 2023 [1]. Among those are wearable IoT devices, which are primarily intended for collecting data, e.g., for patient monitoring, treatment or rehabilitation [2], [3]. Wearable IoT devices are limited in terms of their weight and size and have to satisfy aesthetic requirements [4]. For example, these smart devices are not only designed as

wearable accessories, but also as implants or tattoos and they may be embedded into textiles [2], [3].

Sustainability is a central theme for designing next-generation IoT technology and includes powering IoT devices, such as wearable systems, health monitoring systems, and implants, sustainably [1]. Currently, batteries are considered a hindrance in IoT technology due to the restrictions they impose on devices in terms of, e.g., size, weight, cost, and the need for replacement [1], [5], [6]. Alternative technologies, such as wireless power transfer (WPT) and

energy harvesting (EH), facilitate the operation of battery-free IoT devices [1], [5], [6]. A reliable supply of power to IoT devices can be ensured through the combination of available ambient power sources, such as ambient light, and dedicated power sources [1], [5]. Ambient sources alone can not ensure reliable powering as they are often uncontrollable. In contrast, dedicated power sources, such as dedicated electromagnetic (EM) radiation, offer controllability and thus, can ensure that IoT devices are powered adequately [5].

The acquisition and use of channel state information (CSI) plays a fundamental role in wireless information and power transfer. When the acquisition of CSI is feasible, beamforming-based approaches for directing energy beams towards a multitude of possibly mobile receiver devices are possible. However, the resulting WPT system may be highly complex [1], for example, the WPT system proposed in [7] utilises CSI acquired through uplink training to power devices in the environment. Often, IoT devices are mobile which makes the acquisition of reliable CSI at the transmitter challenging. Moreover, certain types of IoT devices, such as wirelessly powered sensor nodes, may lack the communication capabilities to broadcast pilot symbols, which makes serving EH nodes with power a challenge since focusing energy beams towards them is not possible in a reliable manner due to the missing CSI at the energy transmitter. In this situation, there is a significant risk that the energy beams are misdirected and fail to reach the receivers, leading to an insufficient supply of power to these devices. To ensure the reliable provision of power to an arbitrary number of devices in an environment, the WPT system must be capable of supplying the served environment with a minimum guaranteed level of power at any location without relying on CSI [8], [9].

An essential component for providing a ubiquitous supply of power in an indoor environment is the transmit antenna architecture. Novel antenna architecture designs are being discussed as key enabling technologies for future wireless systems. Advancements beyond massive multiple-input multiple-output (mMIMO) systems include increasing the physical size of antenna arrays and increasing the number of transmit antennas while decreasing the inter-element spacing [10]. In fact, through the incorporation of novel meta-materials, an approximately infinitesimally small inter-element spacing is achieved, allowing to pack almost infinitely many radiating elements into an antenna array, thereby forming a spatially continuous antenna aperture [10]. The technology revolving around these continuous aperture antennas has been coined holographic MIMO (HMIMO) and allows for, e.g., holographic beamforming [11], [12]. HMIMO is being considered as an important technology, e.g., for future 6G wireless communication systems [11]. Moreover, the HMIMO concept is envisioned to offer a seamless and visually appealing integration of antenna arrays into the surfaces of an environment including walls, the ceiling, and even windows [11], [12]. While the benefits

of HMIMO have been demonstrated in the context of communications, the importance of HMIMO for WPT remains unclear.

Indoor wireless systems have been ubiquitous for decades and thus, methods for accurately modelling the wireless channel have been studied extensively. In particular, the frequency range of 2.4 GHz to 5 GHz has received significant attention and thus, deterministic, statistical, and site-specific channel models have been proposed, which differ in accuracy and computational efficiency [13]. In [14], the propagation characteristics of indoor wireless systems operating in the C- and mmWave frequency bands have been investigated for line-of-sight (LoS) and non-line-of-sight (NLoS) scenarios via a software-based ray tracing model. Hereby, the increase in attenuation (path loss) upon increasing the frequency was found to be significantly more severe for the NLoS scenario. Consequently, in the mmWave frequency band, a strong LoS link is required for reliable operation of indoor wireless systems, and due to the severely attenuated scattered components, a LoS channel model is typically adopted [15], [16]. We note that high-frequency systems are attractive for short-range applications, such as indoor WPT [17]. The short wavelength allows the EH antenna of a device to be small [6]. For example, when utilising mmWave frequency bands, mm-scale antennas can be employed [6]. Consequently, the overall size of the devices can be reduced, allowing them to be less obtrusive and easier to integrate, e.g., into fabrics and textiles [1], [5]. Beyond that, a high carrier frequency in conjunction with large antenna architectures, such as, the continuous aperture antennas used in HMIMO, leads to a significant increase in the radiating near-field (Fresnel) region. Although the Fresnel region could typically be neglected in conventional wireless systems, it has to be considered in, e.g., indoor scenarios, for high-frequency systems. Within the Fresnel region, the spherical nature of the EM wavefronts is non-negligible. Adequately capturing the EM wave characteristics in the Fresnel region demands modelling the wireless channel according to the spherical wavefront model (SWM), as the approximation by the planar wavefront model (PWM), typically utilised in the far-field region, does not hold [18]–[20].

Considering the rapidly increasing number of IoT devices [1]–[3], the development of a WPT system, capable of reliably supplying them with power is an important and timely challenge. Emerging technologies, such as HMIMO systems operating in the mmWave frequency band, may play a key role in addressing this problem. Related works have studied the optimisation of the deployment of transmit antennas with the goal of supplying devices with power, e.g., in [21]–[25]. In [21]–[24], operation in the far-field regime is assumed, statistical channel models are adopted, and a coverage area, significantly larger than an indoor space, is considered. For these systems, statistical metrics, such as, outage probability, are utilised for optimising or characterising the positions of power beacons. On the other hand, as

discussed previously, a high operating frequency, such as, in the mmWave frequency band, is affordable and attractive for indoor WPT systems, where a deterministic LoS channel model appropriately characterises the propagation of EM waves. As a consequence of the deterministic channel model, the techniques proposed in [21]–[24] are not applicable and an alternative approach for optimising the deployment of the transmit antennas is required due to the absence of statistical effects. Furthermore, the authors of [25] optimise the location of a finite number of radio stripe elements through geometric programming to maximise the minimum power received by users in indoor energy hotspots in the radiating near-field region. A continuous transmit antenna architecture, as in HMIMO, is precluded as a potential deployment solution when restricting the analysis to a pre-defined number of transmit antennas. Consequently, this leaves the question unanswered whether the novel continuous transmit architecture is beneficial in the context of offering a ubiquitous supply of power in an indoor environment. We aim to address this open point in this work.

In this paper, we propose a multi-user multiple-input single-output (MU-MISO) WPT system, which supplies an entire indoor space with a guaranteed minimum level of power. The transmit antenna architecture of the WPT system is realised via a continuous aperture antenna, which is mounted on the ceiling of a three-dimensional cuboid room. The proposed WPT system can serve an arbitrary number of single-antenna receivers. Assuming free space LoS propagation of the spherical EM wavefronts, we formulate an optimisation problem based on the distance information contained in the amplitude variations of the wireless links between every possible infinitesimally small radiating element and every possible receiver position to determine the optimal distribution of power across the continuous aperture antenna of the transmitter. The objective is to maximise the received power at the worst possible receiver positions in the indoor space. Thus, the proposed solution ensures a reliable supply of power to the receivers, which is a relevant criterion when there is no prior knowledge on the receivers' locations in the room. We establish a connection between the optimal distribution of transmit power and the optimal transmit antenna architecture to study the relevance of emerging HMIMO technology to WPT in an indoor environment. Specifically, employing a continuous aperture antenna would be beneficial if the optimal transmit power distribution's support was found to have the same dimensionality as the distribution's domain. However, if the optimal transmit power distribution's support has a lower dimensionality than its domain, HMIMO technology was not beneficial. The adopted continuous aperture model allows us to capture the full range of transmit antenna architectures ranging from a single transmit antenna to a continuous surface of radiating elements as in HMIMO, thereby enabling a complete analysis of the problem. In contrast, the relevance of HMIMO technology to the considered problem cannot

be adequately studied based on a discrete antenna model. The main contributions of this paper can be summarised as follows:

- We establish a method for investigating the relevance of continuous aperture antennas in the context of offering a ubiquitous supply of power in an indoor environment. To this end, we formulate an optimisation problem for the distribution of a finite amount of transmit power among an uncountable number of radiating elements with the objective of maximising the received signal power at the worst possible receiver position in a given environment.
- We prove that a continuous aperture antenna is unnecessary for the considered problem since our analysis reveals that the support of the optimal distribution of transmit power is a set whose closure has empty interior and Lebesgue measure zero, i.e., the support is shown to have a lower dimensionality than the domain of the transmit power distribution. The support of the optimal distribution corresponds to the optimal positions where transmit antennas should be deployed and we conjecture that the optimal transmit antenna architecture can be realised through a discrete antenna array. In case the transmit antenna architecture is constrained to be one-dimensional, a stronger statement is possible and the optimal number of radiating elements is shown to be finite analytically.
- Through simulation we verify that the optimal transmit power distribution's support is characterised by a finite number of points, and thus, the optimal deployment consists of a finite number of transmit antennas for both one-dimensional and two-dimensional transmit antenna architectures. In the investigated environments, the optimal number of transmit antennas is found to be surprisingly low.
- To validate our findings, the performance of the proposed optimal solution is evaluated against other power allocation schemes. Specifically, we investigate the achievable performance gain of modelling the system in the Fresnel region and we observe that the performance gap compared to the optimal distribution for the far-field operating regime decreases when the worst possible receiver positions in the environment are almost in the far-field. We also show that the loss in performance is low when removing those transmit antennas from the optimal transmit antenna array that are allocated a small amount of transmit power.
- The robustness of the proposed solution is investigated by adding small-scale fading to the LoS link, which leads to a performance loss of less than 2% in the considered environments.

The paper is organised in the following manner. In Section II, the system model is introduced. In Section III, the proposed optimisation problem is formulated and the structure

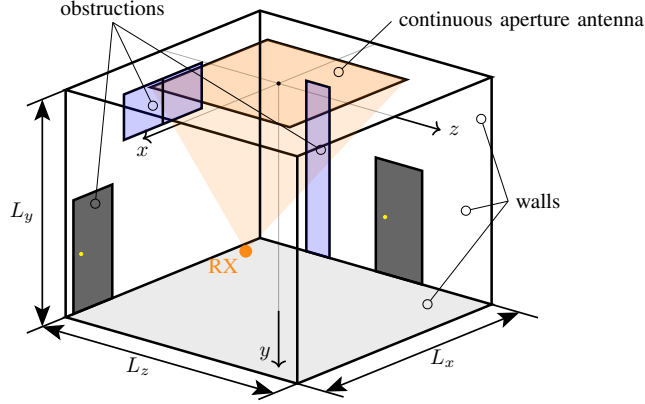


FIGURE 1. Illustration of a three-dimensional environment with a two-dimensional transmit antenna architecture consisting of a continuum of infinitesimally small radiating elements located in a subsection of the x - z plane (orange). The LoS connections of the transmit antenna elements to one receiver (RX) are indicated in orange.

of the optimal distribution of power is determined. As a result, we prove that a finite number of transmit antennas is optimal for the one-dimensional problem and we conjecture that a finite number of transmit antennas is also optimal regarding the two-dimensional problem. In Section IV, we discretise the problem for numerical simulation and, in support of our conjecture, we verify that the optimal number of transmit antennas remains unchanged while increasing the granularity of the sampling grid, i.e., for finer levels of discretisation. In Section V, we provide a performance and sensitivity analysis of our approach, and Section VI concludes this paper.

II. SYSTEM MODEL

The WPT system considered in this paper consists of a transmit antenna architecture employing a continuous aperture antenna and an arbitrary¹ number of single-antenna receivers. Throughout this paper, the terms "transmit antenna" and "radiating element" are used synonymously. An illustration of the considered system is given in Fig. 1, where the transmit antenna architecture is incorporated in the ceiling of a room.

A. ENVIRONMENT

The environment considered in this paper is a three-dimensional cuboid room, where L_x , L_y , and L_z define the size of the environment (see Fig. 1). The origin of the coordinate system is located in the middle of the ceiling of the room. The receivers, e.g., sensors or wearable IoT devices, which may be subject to stringent design requirements, have to be supplied with power wirelessly. To this end, the receivers are considered to be equipped with an antenna for harvesting energy. In this paper, we assume

¹In beamforming-based approaches, such as [7], the number of supported receivers is limited by the number of transmit antennas. In our work, we do not face this restriction since we do not rely on beamforming.

the transmit antenna architecture, which is realised via a continuous aperture antenna, is located on the ceiling. The y -component of the room (see Fig. 1) is defined as the following closed interval in the set of real numbers \mathbb{R}

$$\hat{\mathcal{Y}} = \{y \mid 0 \leq y \leq L_y, L_y > 0\}. \quad (1)$$

The transmit antenna architecture is located at $y = 0$ and is defined in Section II-B. At any other height level of the room, i.e., $y > 0$, there exists a plane $\hat{\mathcal{X}} \times \hat{\mathcal{Z}}$. A receiver location is defined as the triplet $(x_i, y, z_i) \in \hat{\mathcal{X}} \times \hat{\mathcal{Y}} \times \hat{\mathcal{Z}}$ which corresponds to the i -th surface element of $\hat{\mathcal{X}} \times \hat{\mathcal{Z}}$ at height y . The receiver's antenna, which has the finite aperture S_{RX} , is assumed to be centred at (x_i, y, z_i) and to ensure analytical tractability, we assume that the antennas are centred over a lattice defined in $\hat{\mathcal{X}} \times \hat{\mathcal{Z}}$. Therefore, $\hat{\mathcal{X}} \times \hat{\mathcal{Z}}$ is partitioned into disjoint areas of size S_{RX} from which a receiver is capable of harvesting energy. For better legibility, the index i is dropped and a receiver location is written as $(x, y, z) \in \hat{\mathcal{X}} \times \hat{\mathcal{Y}} \times \hat{\mathcal{Z}}$. As a consequence of the position of the origin, $\hat{\mathcal{X}}$ and $\hat{\mathcal{Z}}$ are bounded by $\pm L_x/2$ and $\pm L_z/2$, respectively.

Remark 1: We note that for the problem considered in Section III, the receivers are assumed to lie beyond the reactive near-field of the transmitter, see also Section II-C.

B. TRANSMIT ANTENNA MODEL

In Section I, we have established that high-frequency systems are attractive and affordable for short-range applications, such as indoor WPT [17]. To leverage this, we consider the WPT system to operate in the mmWave frequency band in this paper. Primarily, we consider a two-dimensional transmit antenna architecture. Additionally, we investigate the problem for a one-dimensional transmit antenna architecture which may be preferable in case of obstructions in the area of deployment.

The two-dimensional transmit antenna architecture is deployed on the ceiling, i.e., located in the plane $y = 0$, and is defined as the continuous surface $\mathcal{X}_a \times \mathcal{Z}_a$ comprising an uncountable infinity of infinitesimally small radiating elements with

$$\mathcal{X}_a = \{a_x \mid -L_{a_x}/2 \leq a_x \leq L_{a_x}/2, 0 < L_{a_x} \leq L_x\}, \quad (2)$$

and

$$\mathcal{Z}_a = \{a_z \mid -L_{a_z}/2 \leq a_z \leq L_{a_z}/2, 0 < L_{a_z} \leq L_z\}. \quad (3)$$

By assuming a continuous transmit antenna architecture, no constraint on the minimum size of a radiating element is imposed. The location of an infinitesimally small radiating element is defined by the pair $(a_x, a_z) \in \mathcal{X}_a \times \mathcal{Z}_a$.

Moreover, we assume that the surface, where the antenna architecture is located, i.e., $\mathcal{X}_a \times \mathcal{Z}_a$, is free of obstructions. We note that from a practical point of view, obstructions in the ceiling, such as lights, vents, or sound dampening structures, will prohibit the deployment of excessively large

continuous surfaces in typical indoor environments, such as, an office or a room in a residential building. The radiating elements of the transmit antenna architecture are modelled as identical, omnidirectional antennas. The transmit antenna architecture model $\mathcal{X}_a \times \mathcal{Z}_a$ captures any arrangement of radiating elements ranging from the deployment of a single transmit antenna up to the distribution of radiating elements over a continuous planar surface².

As a special case of this transmit antenna architecture model, we also consider a one-dimensional transmit antenna architecture \mathcal{L}_a with an arbitrary direction in the plane $y = 0$, where the location of a radiating elements is defined as $a_l \in \mathcal{L}_a$, and \mathcal{L}_a is assumed to be continuous.

We note that we neglect the impact of mutual coupling among the transmit radiating elements to ensure analytical tractability of the problem³.

Remark 2: In this paper, we limit our study to transmit antenna architectures deployed on the ceiling of the room, i.e., at $y = 0$. Nevertheless, our results can be extended to the case where the transmit antenna architecture is integrated as part of a wall by exchanging the role of the y -component with the x -component or the z -component.

C. CHANNEL MODEL

In Section I, we discussed that the wireless channel is predominantly LoS in the mmWave frequency band since multipath fading components are weak at such a high frequency. The problem and the proposed solution presented in Section III are developed under LoS conditions. Assuming an LoS channel model allows establishing an intuitive connection between the maximisation of the received power and the geometry underlying the problem. The robustness of the optimal solution is investigated through simulation in Section V, by assuming isotropic scattering in the half-space in front of the transmit antenna architecture in addition to a strong LoS component, based on the Rician fading channel model.

A suitable channel model must capture the propagation characteristics of the EM wavefronts from the transmitter to a receiver accurately. The propagation environment of EM wavefronts can be divided into the near-field and the far-field region. In conventional wireless systems, the near-field region is negligibly small, however, when utilising the mmWave frequency band, which allows the EH antenna of a device to be small, the size of the near-field region becomes

significant. The relationship between the wavelength of the EM waves, the size of the transmit antenna architecture, and the distance between the transmitter and the receiver determines the size of the operating regions [27]. Specifically, a receiver is located within the near-field region if the distance between the receiver and the transmitter is below the Fraunhofer distance $d_{\text{Fraunhofer}} = 2L^2/\lambda$, where L and λ are the antenna's aperture and the wavelength, respectively [27]. The near-field region is further subdivided into the reactive near-field and the radiating near-field region, where the latter is commonly referred to as the Fresnel region. In this paper, we only consider the region beyond the reactive near-field for deployment, i.e., we restrict the receivers not to be located in the reactive near-field of the transmit antenna architecture. The motivation behind this is twofold. Firstly, the size of the reactive near-field region is inherently limited since the deployment of overly large surfaces seems unrealistic (see Section II-B). Secondly, in practice, receivers are unlikely to be located close to the ceiling⁴. The set of receiver positions beyond the reactive near-field is denoted by

$$\mathcal{X} \times \mathcal{Y} \times \mathcal{Z} \subset \hat{\mathcal{X}} \times \hat{\mathcal{Y}} \times \hat{\mathcal{Z}}, \quad (4)$$

and any receiver position (x, y, z) considered in the following satisfies

$$(x, y, z) \in \mathcal{X} \times \mathcal{Y} \times \mathcal{Z}. \quad (5)$$

Therefore, receiver position (x, y, z) lies in the radiating near-field or the far-field region of the transmitter.

For high carrier frequencies, such as in the mmWave band, the reflection and scattering losses are severe, causing the LoS component to be dominant in the wireless channel [18], [28]. Thus, an LoS channel is typically assumed for wireless systems operating in the near-field region [17], [29], [30]. We note that interruptions of the LoS due to obstructions cause blockages [17] and we reduce the risk of channel blockage by placing the transmit antenna architecture on the ceiling of the room instead of on one of the walls (see Section II-B). For the analytical tractability of the system design, we make the assumption that an LoS connection between the radiating elements and the receiver exists and do not consider the impact of channel blockages in this paper. Under free-space LoS conditions, the equivalent complex baseband channel between the radiating element at (a_x, a_z) and a receiver at $(x, y, z) \in \mathcal{X} \times \mathcal{Y} \times \mathcal{Z}$ is given by [27]⁵

$$g_{xyz}(a_x, a_z) = \frac{\sqrt{c}}{D_{xyz}(a_x, a_z)} e^{-j\frac{2\pi}{\lambda} D_{xyz}(a_x, a_z)}, \quad (6)$$

²Note that adopting a discrete transmit antenna model would exclude a continuous planar surface as a possible solution to Problem (14) discussed in Section III. This would preclude the investigation of whether continuous transmit antenna architectures are optimal for maximising the received signal power at the worst possible receiver positions in the environment or not.

³An investigation quantifying the impact of mutual coupling and other reactive near-field effects on system design is an interesting topic for future work. We point out that, in Section IV-C, we show that the optimal deployment only requires a finite number of transmit antennas as illustrated in Fig. 4. We also note that mutual coupling effects are typically neglected for discrete antenna arrays [26, Footnote 4].

⁴We point out that, in Section IV-C, we show that the optimal deployment only requires a finite number of transmit antennas, which is realised with a discrete antenna array, and we illustrate this in Fig. 4.

⁵Including effective aperture losses and polarisation losses and studying their impact on the system performance is an interesting topic for future work. Here, we aim at determining the maximum achievable system performance and focus on providing analytical insights, and thus, we neglect these effects.

where $D_{xyz}(a_x, a_z)$ is the distance between the radiating element at (a_x, a_z) and a receiver at (x, y, z) , i.e., $D_{xyz}(a_x, a_z) = \sqrt{(x - a_x)^2 + y^2 + (z - a_z)^2}$ and c is the channel power gain at the reference distance of 1 meter. By virtue of the spherical nature of the EM wavefronts, both the amplitude and the phase of $g_{xyz}(a_x, a_z)$ depend on distance $D_{xyz}(a_x, a_z)$. In contrast, when the EM wavefronts are modelled as planar waves (far-field approximation), the *path loss*, which is given by the amplitude in (6), between all transmit radiating elements and a receiver is assumed to be constant.

D. TRANSMIT SIGNAL MODEL

We denote the transmit power distribution as P , which is related to the transmit power density p as follows

$$dP(a_x, a_z) = p(a_x, a_z) da_x da_z. \quad (7)$$

The total transmit power is constrained to be finite, i.e.,

$$\iint_{\mathcal{X}_a \times \mathcal{Z}_a} p(a_x, a_z) da_x da_z = \iint_{\mathcal{X}_a \times \mathcal{Z}_a} dP(a_x, a_z) = 1, \quad (8)$$

and, without loss of generality, the transmit power is normalised to unity.

The transmit signal $t(a_x, a_z)$ emitted by the transmit antenna located at (a_x, a_z) is given by

$$t(a_x, a_z) = \sqrt{p(a_x, a_z)} e^{j\theta(a_x, a_z)}, \quad (9)$$

where $p(a_x, a_z) \geq 0$ is the non-negative transmit power density at (a_x, a_z) and $\theta(a_x, a_z)$ is the phase. Since there is no information on the location of the receivers, the transmit signal should illuminate the entire environment. Therefore, the phases are assumed to be independent and identically distributed (i.i.d.) among the radiating elements.

The received signal in position (x, y, z) is given by

$$r_{xyz} = \iint_{\mathcal{X}_a \times \mathcal{Z}_a} t(a_x, a_z) g_{xyz}(a_x, a_z) da_x da_z, \quad (10)$$

and the power of the signal collected by the receiver's antenna with aperture S_{RX} , which is centred at position (x, y, z) , is given by

$$\begin{aligned} \gamma_{xyz} &= S_{RX} \mathbb{E} \left\{ |r_{xyz}|^2 \right\}, \\ &\stackrel{\text{i.i.d.}}{=} S_{RX} \iint_{\mathcal{X}_a \times \mathcal{Z}_a} |t(a_x, a_z) g(a_x, a_z)|^2 da_x da_z, \\ &= c S_{RX} \iint_{\mathcal{X}_a \times \mathcal{Z}_a} \frac{p(a_x, a_z)}{[D_{xyz}(a_x, a_z)]^2} da_x da_z, \end{aligned} \quad (11)$$

where $\mathbb{E}\{\cdot\}$ denotes the expectation operator and we exploit that the phases $\theta(a_x, a_z)$ are i.i.d. Therefore, the power received by the receiver in position (x, y, z) is directly proportional to

$$\Phi_P \{f_{xyz}(a_x, a_z)\} = \iint_{\mathcal{X}_a \times \mathcal{Z}_a} f_{xyz}(a_x, a_z) dP(a_x, a_z), \quad (12)$$

with

$$f_{xyz}(a_x, a_z) = \left(\frac{1}{D_{xyz}(a_x, a_z)} \right)^2. \quad (13)$$

Operator $\Phi_P\{\cdot\}$ represents the integration of function $f_{xyz}(a_x, a_z)$ with respect to (w.r.t.) the transmit power distribution P . Mathematically, this is equivalent to the expectation of a function $f_{xyz}(a_x, a_z)$ w.r.t. a probability distribution. This equivalence is crucial and it will be exploited in Section III-C, where we will leverage the mathematical equivalence between determining the optimal transmit power distribution across a continuous aperture antenna, which we study in this paper, and the problem of finding the capacity-achieving amplitude-constrained input distribution of a channel, which has been studied in, e.g., [31]–[33]. Note that the impact of additive noise on the received power is neglected in (11), (12). Furthermore, we note that the amount of power harvested by a device is a non-decreasing function of the received signal power [34].

III. OPTIMAL TRANSMIT POWER DISTRIBUTION

Our goal is to supply power to an arbitrary number of receivers in the environment without any knowledge of their location. This objective can be achieved by maximising the received signal power for the worst possible receiver position(s) in the environment, which leads to a max-min optimisation problem. In this section, we formulate this optimisation problem to optimise the transmit power distribution P . Hereby, the optimal transmit power distribution P^* characterises the optimal transmit antenna architecture. Deploying an HMIMO system would be necessary if we found that the optimal transmit power distribution's support had the same dimensionality as the distribution's domain. However, we will prove in Section III-C that the optimal transmit power distribution's support has a lower dimensionality than the distribution's domain and thus, a HMIMO system is unnecessary in the context of the considered WPT problem.

A. PROBLEM FORMULATION

Maximising the power at the receiver's antenna centred at point $(x, y, z) \in \mathcal{X} \times \mathcal{Y} \times \mathcal{Z}$ in the environment is achieved by maximising $\Phi_P\{f_{xyz}\}$, defined in (12), via an optimal distribution of transmit power among the radiating elements, where P is a member of the set of distributions Ω , i.e., $P(a_x, a_z) \geq 0, \forall (a_x, a_z) \in \mathcal{X}_a \times \mathcal{Z}_a$, and (8) is satisfied. Hereby, the non-negativity and finite power constraints, which have been introduced in Section II-B, apply to every element of Ω . Moreover, the function $P(a_x, a_z)$ is restricted to the set $\mathcal{X}_a \times \mathcal{Z}_a$, and as a consequence of (8), $P(a_x, a_z)$ is bounded by one and thus, is square-integrable. Therefore, the set of considered distributions Ω is a subset of the square-integrable (finite energy) functions defined over the transmit antenna domain and denoted as $\mathcal{L}^2(\mathcal{X}_a \times \mathcal{Z}_a)$, i.e., $P(a_x, a_z) \in \Omega \subset \mathcal{L}^2(\mathcal{X}_a \times \mathcal{Z}_a)$. The set Ω is further characterised in the following lemma.

Lemma 1. *The set of distributions $\Omega \subset \mathcal{L}^2(\mathcal{X}_a \times \mathcal{Z}_a)$ is a weakly compact space in the weak topology and convex.*

Proof: The proof is found in Appendix A.

Ensuring that receivers are reliably supplied with power is achieved by maximising the received signal power at the worst possible receiver position(s). This can be formulated as the following max-min optimisation problem

$$\underset{P \in \Omega}{\text{maximise}} \quad \underset{\substack{(x,y,z) \\ \in \mathcal{X} \times \mathcal{Y} \times \mathcal{Z}}}{\min} \quad \Phi_{P^*}\{f_{xyz}\}. \quad (14)$$

The best worst-case performance, i.e., the optimal objective value of Problem (14), is denoted by m and is defined as

$$m = \underset{\substack{(x,y,z) \\ \in \mathcal{X} \times \mathcal{Y} \times \mathcal{Z}}}{\min} \quad \Phi_{P^*}\{f_{xyz}\}, \quad (15)$$

where P^* is the optimal distribution of power. Note that Problem (14) is linear in P . The feasibility of Problem (14) is ensured through the compactness of Ω shown in Lemma 1, i.e., Ω is closed and bounded.

B. CRITICAL RECEIVER POSITIONS

By identifying the receiver locations where the received signal power is the lowest, the complexity of solving Problem (14) can be reduced. These critical locations are defined w.r.t. the optimal distribution of power P^* . To this end, the set containing the critical receiver positions when power is allocated optimally is denoted by $\mathcal{R}_{\text{crit}}$. The set of non-critical positions is the complement of $\mathcal{R}_{\text{crit}}$, i.e., $\mathcal{R}_{\text{crit}}^c$. After the power has been optimally allocated across the continuous transmit antenna surface, the signal power received by an antenna centred at a critical receiver position $(x, y, z) \in \mathcal{R}_{\text{crit}}$ will be below the signal power received by an antenna centered at any non-critical location $(x, y, z) \in \mathcal{R}_{\text{crit}}^c$. Next, the set of critical receiver positions is characterised more precisely.

Key Observation 1. *For any $(x, z) \in \mathcal{X} \times \mathcal{Z}$, the worst performance is attained at $y = L_y$. Consequently, all critical positions are located at $y = L_y$, i.e., $\mathcal{Y}_{\text{crit}} = \{L_y\}$.*

Key Observation 1 holds since f_{xyz} is a monotonically decreasing function of y . Thus, the lowest objective value is obtained in the plane with $y = L_y$. As a consequence of Key Observation 1⁶, the function f_{xyz} in the objective function of Problem (14) can be equivalently substituted by $f_{xz}(a_x, a_z) := f_{xyz}(a_x, a_z)|_{y=L_y}$. Problem (14) is equivalently reformulated in the following lemma.

Lemma 2. *Assume that the set of critical positions $\mathcal{R}_{\text{crit}} \subseteq \mathcal{X} \times \mathcal{Y}_{\text{crit}} \times \mathcal{Z}$ is known. Then, solving Problem (14) is*

⁶Note that the result in Key Observation 1, i.e., $\mathcal{Y}_{\text{crit}} = \{L_y\}$, holds since the radiating elements are assumed to be omnidirectional antennas and dropping this assumption may change the result.

equivalent to solving the following problem

$$\underset{o \in \mathbb{R}, P \in \Omega, \Lambda}{\text{maximise}} \quad o - \underbrace{\sum_{\mathcal{R}_{\text{crit}}} (o - \Phi_P\{f_{xz}\}) \lambda_{xz}}_{J(P)}, \quad (16)$$

where Λ is the set of positive variables $\lambda_{xz} > 0, \forall (x, y, z) \in \mathcal{R}_{\text{crit}}$. When allocating power optimally through $P^*(a_x, a_z)$, the optimal objective value is $o^* = m$ and the following conditions should also hold

$$\begin{aligned} &[(\lambda_{xz} > 0 \implies m = \Phi_{P^*}\{f_{xz}\}) \text{ or} \\ &(m < \Phi_{P^*}\{f_{xz}\} \implies \lambda_{xz} = 0)], \\ &\forall (x, y, z) \in \mathcal{X} \times \mathcal{Y}_{\text{crit}} \times \mathcal{Z}. \end{aligned} \quad (17)$$

Proof: The proof is presented in Appendix B.

The objective function in Problem (16) is referred to as $J(P)$ in the following. Note that Problem (14) is a convex optimisation problem, which is readily apparent when the problem is stated in its epigraph form [35] (see Appendix B).

C. OPTIMAL STRUCTURE OF POWER DISTRIBUTION

In this section, we establish a relation between Problem (16) and the problem of finding the optimal amplitude-constrained input distribution for reaching the information capacity of Gaussian channels studied in [31]–[33]. In [31] and [32], the authors determine the optimal input distribution of transmit symbols, which are bounded in amplitude, for achieving information capacity, whereas our problem lies in identifying the optimal distribution of transmit power, under geometrical constraints regarding the continuous transmit antenna architecture. Beyond communication problems [31], similar results on the optimal input distribution in WPT applications have been established in [32]. First, we consider the optimisation of a two-dimensional distribution $P(a_x, a_z)$ which is significantly different from the problems involving one-dimensional distributions such as [31] and [32]. Specifically, the properties of the optimal two-dimensional distribution's structure are less stringent. The analysis of optimisation problems involving input distributions with a dimensionality greater than one has been studied in [33]. Subsequently, we consider the optimisation problem with a one-dimensional distribution, which allows characterising the optimal distribution as in [31] and [32].

In the following, we investigate properties, which apply to the optimal distribution of power and allow the characterisation of the optimal transmit antenna architecture. The main results are stated in Propositions 2 and 3 for the optimal distribution of power over a two-dimensional surface and in Proposition 4 for the optimal one-dimensional distribution. First, a necessary and sufficient condition for the optimal distribution of power P^* is established in Proposition 1 and Corollary 1.

Proposition 1. *Consider the optimisation problem in (16). There exists an optimal distribution of power $P^*(a_x, a_z)$*

which attains the maximum m of Problem (16) if and only if the following condition holds

$$\iint_{\mathcal{X}_a \times \mathcal{Z}_a} \bar{f}(a_x, a_z) dP(a_x, a_z) \leq m, \quad \forall P \in \Omega, \quad (18)$$

where $\bar{f}(a_x, a_z)$ is given by

$$\bar{f}(a_x, a_z) = \frac{\sum_{\mathcal{R}^{\text{crit}}} f_{xz}(a_x, a_z) \lambda_{xz}}{\sum_{\mathcal{R}^{\text{crit}}} \lambda_{xz}}, \quad (19)$$

and (18) is satisfied with equality for the optimal distribution of power $P^*(a_x, a_z)$.

Proof: This proposition is proven in Appendix C.

Intuitively, function \bar{f} can be interpreted as the weighted average of f_{xz} over the receiver positions $\mathcal{X} \times \mathcal{Z}$ at $y = L_y$. The weights are given by the variables $\lambda_{xz} / \sum_{\mathcal{R}^{\text{crit}}} \lambda_{xz}$ and thus, only critical receiver positions contribute to \bar{f} . Note that the optimal distribution P^* is not necessarily unique since $J(P)$ is linear in P and not strictly concave as in the problems considered in [31], [32]. Additionally, Proposition 1 provides a condition for the existence of P^* . Obtaining P^* requires determining the variables λ_{xz} satisfying (18) and (19).

Next, the optimality condition for P^* , given in Proposition 1, is restated in a more intuitive manner. This requires defining the support of P^* , which is analogous to the definition in [33]. A radiating element's position (a_x, a_z) is called a *point of increase* of the optimal distribution P^* if for any open subset $O \subset \mathbb{R}^2$ containing (a_x, a_z) , $P^*(O) > 0^7$ holds [33]. The set of points of increase of P^* is defined as $\mathcal{E}(P^*) \subseteq \mathbb{R}^2$. Note that $P^*(\mathcal{E}(P^*)) = 1$ [33]. Moreover, $\mathcal{E}(P^*)$ is the smallest closed subset of \mathbb{R}^2 such that $P^*(\mathcal{E}(P^*)) = 1$ [33]. Note that $P \in \Omega$ is restricted to $\mathcal{X}_a \times \mathcal{Z}_a \subset \mathbb{R}^2$ and thus, $\mathcal{E}(P^*) \subseteq \mathcal{X}_a \times \mathcal{Z}_a$. We define $\mathcal{E}(P^*)$ as the support of P^* .

Corollary 1. Consider the optimisation problem in (16). There exists an optimal distribution of power P^* for Problem (16) if and only if $\bar{f}(a_x, a_z)$ satisfies the following equations

$$\bar{f}(a_x, a_z) \leq m, \quad \forall (a_x, a_z) \in \mathcal{X}_a \times \mathcal{Z}_a, \quad (20)$$

$$\bar{f}(a_x, a_z) = m, \quad \forall (a_x, a_z) \in \mathcal{E}(P^*). \quad (21)$$

Proof: The proof is provided in Appendix D.

Thus, Corollary 1 describes the relationship between the optimal distribution of transmit power P^* for attaining the optimal objective value m of Problem (16) and the optimal set of positions regarding the radiating elements $\mathcal{E}(P^*)$, i.e., the support of P^* .

Based on the optimality conditions on P^* defined in Proposition 1 and Corollary 1, the set of optimal positions regarding the radiating elements is characterised more precisely. First, we complete our analysis of the two-dimensional distribution $P^*(a_x, a_z)$. Subsequently, we characterise the set of optimal positions under the constraint of

⁷Here, the argument of the optimal transmit power distribution is a set instead of a tuple of points, i.e., $P^*(O)$ corresponds to $\iint_O dP^*(a_x, a_z)$.

a continuous one-dimensional deployment. The characterisation requires the following definition in the two-dimensional scenario.

Definition 1 (see [33]). A subset $S_1 \subset S_0$ is dense in S_0 if every element $s \in S_0$ is either an element of S_1 or an accumulation point of S_1 . A subset $S_1 \subset S_0$ is nowhere dense if $S_2 \cap S_1$ is not dense in S_0 , where S_2 is any non-empty open set $S_2 \subset S_0$.

Proposition 2. The support $\mathcal{E}(P^*) \subset \mathcal{X}_a \times \mathcal{Z}_a$ of the optimal two-dimensional distribution of power P^* is a nowhere dense set of $\mathcal{X}_a \times \mathcal{Z}_a$.

Proof: The proof is provided in Appendix E.

Proposition 3. The support $\mathcal{E}(P^*) \subset \mathcal{X}_a \times \mathcal{Z}_a$ of the optimal two-dimensional distribution of power P^* is of Lebesgue measure zero.

Proof: The proof is provided in Appendix F.

Thus, $\mathcal{E}(P^*)$ is a set of pairs (a_x, a_z) , which define the optimal positions of radiating elements, that is nowhere dense and has Lebesgue measure zero, i.e., the set $\mathcal{E}(P^*)$ does not occupy any measurable surface in $\mathcal{X}_a \times \mathcal{Z}_a$. Intuitively, the set $\mathcal{E}(P^*)$ could consist of isolated points scattered throughout $\mathcal{X}_a \times \mathcal{Z}_a$ since both properties hold in this case. On the other hand, Propositions 2 and 3 do not preclude the possibility of $\mathcal{E}(P^*)$ containing more complex structures, such as continuous one-dimensional structures, as long as $\mathcal{E}(P^*)$ is nowhere dense and of measure zero. This is further investigated in Section IV. We note that based on Propositions 2 and 3, a continuous planar transmit antenna architecture, which is utilised in HMIMO, is unnecessary for WPT. Moreover, observe that, by virtue of the max-min problem, the optimal distribution must be symmetrical w.r.t. the x -axis and the z -axis, i.e., $P^*(a_x, a_z) = P^*(-a_x, a_z) = P^*(-a_x, -a_z) = P^*(a_x, -a_z)$. Violating this symmetry condition would lead to a decrease in performance at the worst possible receiver positions, i.e., a decrease of the objective value.

The results presented in this section, which allowed drawing conclusions regarding the optimal deployment of transmit radiating elements $\mathcal{E}(P^*)$, pertained to the analysis of a two-dimensional distribution of power. In the following, we restrict the continuous transmit antenna architecture to lie on the one-dimensional set \mathcal{L}_a , which results in a problem analogous to [31], [32] (see Section B). Consequently, the optimal distribution of power $\tilde{P}^*(a_l)$ along \mathcal{L}_a is one-dimensional. This problem is investigated in the following, whereby the optimal set of positions of the radiating elements $\tilde{\mathcal{E}}(\tilde{P}^*) \subset \mathcal{L}_a$ is shown to be finite.

Proposition 4. The support $\tilde{\mathcal{E}}(\tilde{P}^*) \subset \mathcal{L}_a$ of the optimal one-dimensional distribution is a finite set of points.

Proof: The proof is provided in Appendix G.

We note that a continuous transmit antenna architecture is unnecessary for one-dimensional transmit antenna architectures since Proposition 4 guarantees that a finite number of radiating elements is sufficient.

IV. SYSTEM DISCRETISATION

In the following, to shed light on our analytical results in Section III, the optimal transmit antenna architecture is studied via numerical analysis. In order to solve Problem (14) numerically, the continuous sets $\mathcal{X}_a \times \mathcal{Z}_a$ and \mathcal{L}_a have to be discretised. For a one-dimensional transmit antenna architecture, we have proven in Proposition 4 that a finite number of transmit antennas placed in $\tilde{\mathcal{E}}(\tilde{P}^*) \subset \mathcal{L}_a$ is optimal. For a two-dimensional transmit antenna architecture, Proposition 3 guarantees that the optimal deployment of transmit antennas is on a set $\mathcal{E}(P^*) \subset \mathcal{X}_a \times \mathcal{Z}_a$ with Lebesgue measure zero. We obtain approximations of the optimal solution to Problem (14) through discretising the problem, and subsequently, solving it numerically. We verify numerically that the solution of the optimisation problem remains unchanged for finer levels of discretisation (LoD), i.e., for an increasing granularity of the sampling grid. Further, since Propositions 2 and 3 ensure that the optimal set of transmit antennas $\mathcal{E}(P^*) \subset \mathcal{X}_a \times \mathcal{Z}_a$ is nowhere dense and has Lebesgue measure zero, which are properties satisfied by a set of isolated points scattered within $\mathcal{X}_a \times \mathcal{Z}_a$, we conjecture that such a set of isolated points is optimal. Thereby, to support this conjecture by simulation results, it is necessary to investigate whether the number of transmit antennas increases monotonically for finer LoD or if the number of transmit antennas remains constant. Intuitively, if the latter is true, there is an optimal, finite number of transmit antennas, which depends on the geometrical properties of the environment, i.e., L_x , L_y , and L_z , at least from a practical point of view. The three-dimensional environments, which are investigated in this paper, are listed in Table 1. The difference between the environments is the ratio of height to width since the width and depth of the room are chosen to be equal. The environments are denoted by their height-to-width ratio. We note that the dimensions of the environments

TABLE 1. Definition of the four environments analysed in Sections IV and V.

Height L_y in [m]	Width L_x in [m]	Depth L_z in [m]	Height Width
2	2	2	1/1
2	6	6	1/3
2	8	8	1/4
2	10	10	1/5

listed in Table 1 are realistic, e.g., for an office or a room in a residential building. In environments spanning a significantly larger area, such as, a factory building, mmWave operating frequencies become unaffordable due to the large path loss, which would result in a very low received power when

receivers are located far away from a transmitter, and thus, operation at a lower frequency would be preferred. However, NLoS components become increasingly important for decreasing operating frequency, and thus, the wireless channel may not be accurately described by a deterministic LoS channel. In this case, it is preferable to consider alternative wireless systems and models, such as those in [21]–[24], for which optimal transmit antenna deployment and power allocation differ significantly in methodology and solutions.

A. DISCRETISED OPTIMISATION PROBLEM

In the following, the set of transmit antenna positions, i.e., $\mathcal{X}_a \times \mathcal{Z}_a$ for the two-dimensional problem and \mathcal{L}_a for the one-dimensional problem, is discretised. In this paper, we only investigate systems where the discretised transmit antenna architecture, which we also refer to as a (discrete) antenna array, covers the entire ceiling⁸, i.e., $L_{a_x} = L_x$ and $L_{a_z} = L_z$. The one-dimensional antenna array is also placed on the ceiling along the x -axis, i.e., $\mathcal{L}_a = \mathcal{Z}_a$. Moreover, we set $L_x = L_z$. The LoD is defined as the number $N + 1$ of equally-sized intervals into which the sets \mathcal{X}_a , \mathcal{Z}_a and \mathcal{L}_a are partitioned, respectively. Consequently, we have a grid of antenna positions with $(N + 1)^2$ elements in $\mathcal{X}_a \times \mathcal{Z}_a$ and $N + 1$ elements in \mathcal{L}_a , respectively. The position of transmit antenna i , which corresponds to one element of the grid, is given as $(a_x, a_z)_i$, with $i = 1, \dots, (N + 1)^2$, in two dimensions and $(a_l)_i$, with $i = 1, \dots, N + 1$, in one dimension. In the following, the coordinates of position $(a_x, a_z)_i$ are denoted by a_{xi} and a_{zi} . Similarly, the coordinate of position $(a_l)_i$ is given by a_{li} . By utilising the definitions in Section II-D, Problem (14) is discretised as follows

$$\underset{o \in \mathbb{R}, p(a_{xi}, a_{zi})}{\text{maximise}} \quad o \quad (22a)$$

$$\text{subject to} \quad o \leq \sum_{(a_{xi}, a_{zi})} f_{xz}(a_{xi}, a_{zi}) p(a_{xi}, a_{zi}),$$

$$\forall (x, L_y, z) \in \mathcal{X} \times \mathcal{Y}_{\text{crit}} \times \mathcal{Z}, \quad (22b)$$

$$\sum_{(a_{xi}, a_{zi})} p(a_{xi}, a_{zi}) = 1, \quad (22c)$$

$$p(a_{xi}, a_{zi}) \geq 0, \quad (22d)$$

where the problem has been rewritten in epigraph form [35]. After discretisation, the convex optimisation problem in (22) can be solved efficiently, for example, by applying the interior-point method [35]. The problem is solved using standard numerical tools for convex optimisation, such as CVXPY [36], [37]. For all results shown, any value below 10^{-6} in the optimal distribution of power was deemed to a representation and computation error in computer arithmetics and was set to zero. In the worst case, values below 10^{-6}

⁸In Section II-B, the deployment of excessively large continuous surfaces in typical indoor environments was deemed unsuitable due to obstructions in the ceiling. This problem is substantially less severe when deploying discrete transmit antennas within $\mathcal{X}_a \times \mathcal{Z}_a$ or \mathcal{L}_a as considered in this section.

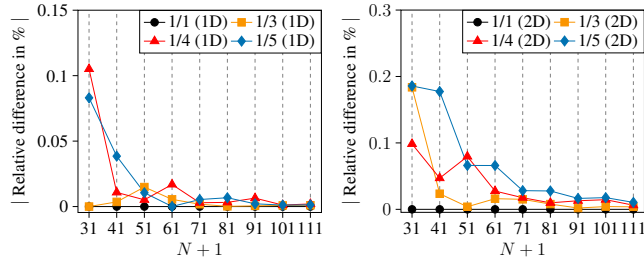


FIGURE 2. Absolute value of relative difference between objective values in percent for increasing N for the height-to-width ratios defined in Table 1.

accounted for less than $10^{-5}\%$ of the total power distributed among the transmit antennas.

B. LEVEL OF DISCRETISATION

There is an inherent trade-off between the computational complexity of solving a problem and the accuracy of its solution. The necessary LoD is determined based on a desired accuracy and a criterion to assess whether the proposed solution is sufficiently accurate. To this end, Problem (22) was solved repeatedly for increasing granularity of the sampling grid. Subsequently, the differences between the objective values of consecutive iterations were evaluated.

In Fig. 2, the absolute value of the relative difference between the objective values, i.e., the absolute value of the difference between the current and previous objective value divided by the current objective value, was calculated for every N . As the LoD increases, the accuracy increases for all investigated environments since the objective value stabilises. From Fig. 2, at LoD $N + 1 = 81$, the relative difference lies below 0.05% and beyond that, the improvements were deemed negligible. Consequently, unless specified otherwise, all simulations in the following are performed at LoD $N + 1 = 81$.

C. FINITENESS OF OPTIMAL POWER DISTRIBUTION

In this section, the optimal number of transmit antennas⁹ N_t^* is investigated for increasing LoD. To this end, the optimal number of transmit antennas for each considered environment is displayed in Fig. 3. In Fig. 3, one can observe that the optimal number of transmit antennas N_t^* does not increase monotonically for different LoDs, which suggests that a finite number of antennas is indeed optimal, even for a two-dimensional array. The optimal number of antennas to be deployed depends on the geometry of the environment and the dimensionality of the transmit antenna architecture. We note that in Section III, the optimal solution of the problem is characterised in the context of a continuous architecture and a slight mismatch between the optimal positions regarding the continuous architecture and the optimal positions regarding the discretised architecture

⁹The optimal number of transmit antennas is defined as the number of non-zero values in the solution $p^*(a_{ix}, a_{iz})$ of Problem (22).

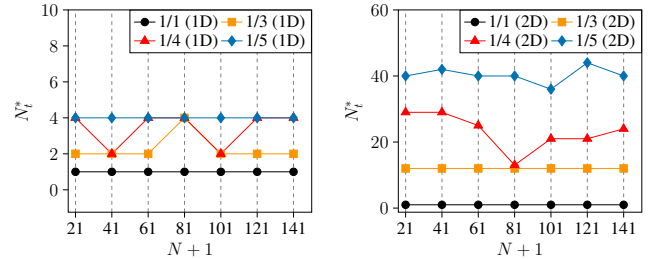


FIGURE 3. Optimal number of transmit antennas, i.e., number of positions where non-zero powers are allocated by the optimal distribution, for increasing N for the height-to-width ratios given in Table 1.

may occur depending on how well the optimal solution can be embedded in the grid at a certain granularity (see Section V-A). Consequently, slight fluctuations regarding the optimal number of transmit antennas are expected, which are visible in Fig. 3. However, note that these fluctuations are negligible compared to the difference in the number of grid cells among different LoDs, especially for the two-dimensional array with $(N + 1)^2$ cells.

In general, the optimal number of transmit antennas is larger when employing a two-dimensional antenna array compared to the deployment over a one-dimensional transmit antenna array. Moreover, for a decreasing height-to-width ratio, the optimal number of transmit antennas increases, especially when employing a two-dimensional antenna array.

V. PERFORMANCE AND SENSITIVITY ANALYSIS

We assume a LoD of $N + 1 = 81$, a transmit power of 10 W, $S_{RX} = \lambda^2/4$, which is on the scale of the antenna aperture proposed in [38], and a wavelength of $\lambda = 12.5$ mm for the considered system¹⁰.

Next, we evaluate the boundaries of the near-field region in the context of the discretised antenna array. The room is contained within $d_{\text{Fraunhofer}}$ since the antenna architecture covers the entire ceiling, which has a side length of at least the height of the room. Reactive near-field effects are typically limited to a short distance around the individual

¹⁰A wavelength of $\lambda = 12.5$ mm corresponds to an operating frequency of 24 GHz, which is at the low end of the mmWave frequency band [6]. The electromagnetic field (EMF) radiation exposure limit for the proposed system operating at 24 GHz is around 9.9 W/m^2 [39]. Considering the worst-scenario, i.e., when only a single transmit antenna is deployed which radiates a power of 10 W, the minimum distance d_{min} from the single antenna to be below the exposure limit is around $d_{\text{min}} = \sqrt{10 \text{ W}/(4\pi \cdot 9.9 \text{ W/m}^2)} \approx 0.28$ m. The exposure to EMF radiation decreases for an increasing distance between the transmit antenna array and the receiver [39]. When the transmit power is spread across multiple antennas, which is optimal for the majority of considered environments as shown in Fig. 4, the required distance from the ceiling to be below the exposure limit reduces. In our system, the transmit antenna array is positioned on the ceiling of the environment and thus, from a practical point of view, the EMF exposure to humans in the environment will typically be below the required limit since they will have a certain distance to the ceiling.

radiating elements in the context of discrete antenna architectures [26], [40]. Specifically, reactive near-field effects are negligible beyond a distance of $d_{\text{Fresnel}} = \sqrt[3]{\frac{L_{\text{element}}^4}{8\lambda}}$ from an antenna element with aperture L_{element} , which is typically on the order of the wavelength. Thus, d_{Fresnel} is typically limited to a few wavelengths from the transmit antenna [27], [40].

A. HEATMAPS OF OPTIMAL DISTRIBUTIONS

The solution $p^*(a_{xi}, a_{zi})$ of Problem (22) is visualised in Fig. 4 using heatmaps for the height-to-width ratios considered in Table 1. The value zero is depicted using white colour, while the non-zeros are represented by a colour corresponding to the percentage of power allocated to the position. Thus, transmit antennas are represented by a colour different from white.

This depiction supports our conjecture that the optimal transmit antenna positions are isolated points. Except for a height-to-width ratio of one, the room is contained within the near-field of the optimal antenna deployment since the largest distance between individual transmit antennas defines the aperture of the array generated by the antennas [40]. From a practical point of view, the proposed optimal deployment may be realised via a distributed antenna system.

For a height-to-width ratio equal to one, it is optimal to place a single antenna in the centre of the ceiling. In this case, the proposed system does not have to be optimised for operating in the Fresnel region since the critical receiver positions, which are in the corners of the room at $y = L_y$, are in the far-field in this scenario.

B. MINIMUM RECEIVED POWER AND COMPARISON TO ALTERNATIVE DEPLOYMENTS

In this section, the performance of the proposed optimal two-dimensional distribution of power is measured in terms of the minimum received power in the environment. This value corresponds to the guaranteed level of received power, which is available at any single receiver position (x, y, z) beyond the reactive near-field region of the room. Thus, we display the performance of the worst-case scenario, which applies to a subset of receiver positions at the floor $y = L_y$ of the room since the antennas are deployed on the ceiling.

The proposed optimal method is denoted by M-OPT. Moreover, the performance is compared to other power allocation methods, which are listed below:

- The achievable performance gain of modelling the system in the Fresnel region is highlighted by comparing the proposed approach to the optimal power distribution designed under the far-field approximation. By virtue of the max-min problem, under the far-field assumption, the ideal deployment location lies in the centre of the ceiling since the path losses corresponding to different transmit antennas are assumed to be identical. As a consequence of the constant path loss, a single transmit

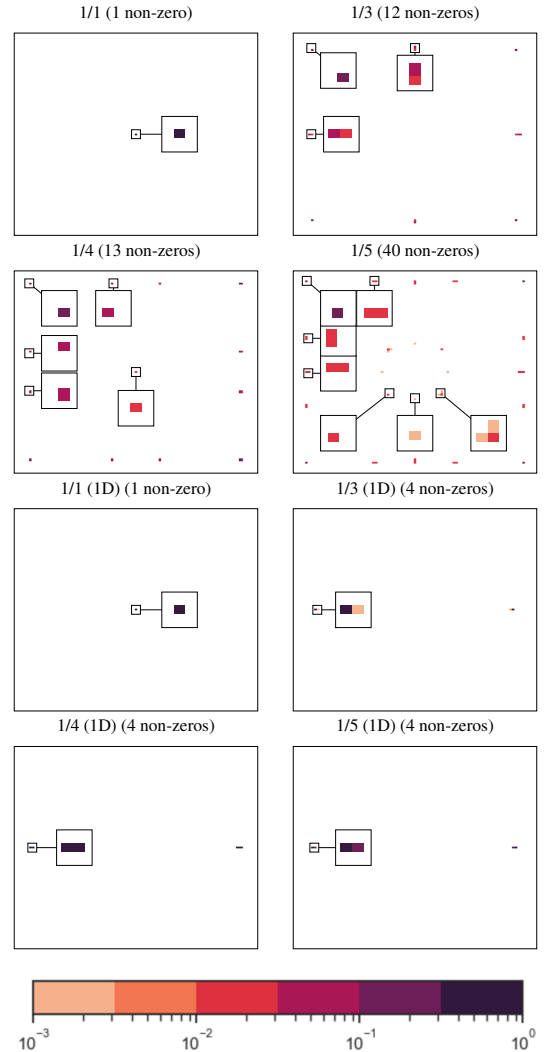


FIGURE 4. Heatmaps of optimal power distributions for the height-to-width ratios listed in Table 1 with $N + 1 = 81$. Each heading indicates the height-to-width ratio from Table 1, the dimensionality of the transmit antenna array, and the number of non-zeros of $p^*(a_{ix}, a_{iz})$ in brackets, i.e, the optimal number of transmit antennas. The relative amount of power allocated to an antenna is colour-coded according to the colour bar at the bottom. The antennas are partly magnified to aid visualising the solution. The colours of the unmagnified antennas follow from the symmetry of the optimal solution discussed in Section III.

antenna is deployed to which all the available power is allocated. This benchmark scheme is referred to as M-FF.

- A uniform power distribution across the antenna array, where an antenna is located at every grid cell and the power is split equally among the antennas. This benchmark scheme is referred to as M-UNI.
- We derive a suboptimal scheme from the proposed optimal approach by removing optimally deployed transmit antennas operating with low transmit power. Thereby, small non-zero values are set to zero in the distribution, and subsequently, the allocated powers are re-normalised for a fair comparison at equal total transmit power. More specifically, the x -th percentile of

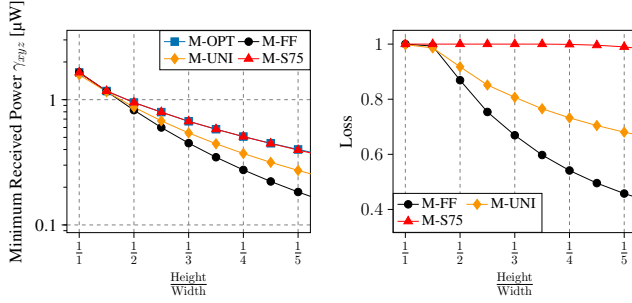


FIGURE 5. Minimum received power at the worst location in the environment and loss of the benchmark schemes and suboptimal schemes compared to proposed optimal deployment and power allocation. The height is fixed at 2 m.

the allocated power levels was calculated and transmit antennas operating at a power level lower than the one corresponding to the x -th percentile were removed, followed by the re-normalisation of power. We investigated the 75th, percentile of the non-zero values. The scheme is referred to as M-S75.

We present the performance results in Fig. 5. Hereby, we investigate the performance by evaluating the minimum received power¹¹, i.e., the power at the critical receiver positions, for M-OPT, M-FF, M-UNI, and M-S75 for environments with different height-to-width ratios. Moreover, we determine the performance loss incurred by utilising M-FF, M-UNI, and M-S75 in comparison to the proposed optimal scheme M-OPT. To this end, we calculate the loss compared to the proposed optimal solution by dividing the objective value of a benchmark scheme, i.e., M-FF or M-UNI, or the suboptimal scheme, i.e., M-S75, by the objective value obtained through the optimal deployment and power allocation, i.e., the solution of Problem (22), i.e., M-OPT.

For all schemes, we observe that the minimum received power decreases for a decreasing height-to-width ratio. This effect occurs due to the increasing environment size for decreasing height-to-width ratio while keeping the total transmit power constant. Note that the received power can be increased by adding more receive antennas or increasing the receiver's antenna size S_{RX} .

We observe that the proposed optimal power distribution outperforms or matches the performance of the other schemes. For a height-to-width ratio of one, we see from Fig. 4 that the proposed optimal solution coincides with M-FF and we find no performance loss between M-OPT and the other schemes. On the other hand, for decreasing height-to-width ratio the performance gap between M-OPT and the alternative methods grows. We observe the largest performance

¹¹Typical EH circuits are designed for receive powers in the μW range [41]. The constantly available and guaranteed received power is in the range of, e.g., the continuous standby power required by the nanowatt sensors presented in [42]. Moreover, receivers capable of receiving energy at multiple positions, e.g., through multiple receiving antennas can increase the amount of received power.

gap between M-OPT and M-FF which indicates the relevance of accurately modelling the wireless channel by taking into account the spherical EM wavefronts when operating in the near-field region. Moreover, a uniform distribution of power, i.e., in the case of M-UNI, is also found to be highly suboptimal, especially for small height-to-width ratios. On the other hand, the loss in performance compared to the optimal distribution is negligible for M-S75 with a slight loss observable for a height-to-width ratio of 1/5. This is because antennas radiating a relatively low amount of power contribute little to the minimum received power. Therefore, removing these transmit antennas comes at a small loss in received power for the investigated environments.

C. SENSITIVITY ANALYSIS

While the assumption of a strong LoS channel, which was made throughout this paper, is valid for very high carrier frequencies, a low-power small-scale fading component may still be present. This requires including an NLoS component in the wireless channel model [43]. Assuming isotropic scattering, the NLoS component can be modelled as spatially correlated Rayleigh fading [44], [45], [46]. The superposition of the NLoS and LoS components is modelled by a Rician fading channel.

In this section, we assess the robustness of the proposed optimal two-dimensional power distribution in the presence of scattering objects in the environment using a Rician fading channel model. The Rician fading channel between transmit antenna i and the receiver position (x, L_y, z) is defined as

$$\tilde{g}_{xz}(a_{xi}, a_{zi}) = \sqrt{\frac{\kappa}{\kappa + 1}} g_{xz}(a_{xi}, a_{zi}) + \sqrt{\frac{1}{\kappa + 1}} h(a_{xi}, a_{zi}), \quad (23)$$

where constant κ denotes the Rician K -factor and the LoS channel is given in (6). The NLoS channel vector $\mathbf{h} = [h(a_{x1}, a_{z1}), \dots, h(a_{x(N+1)^2}, a_{z(N+1)^2})]^T \in \mathbb{C}^{(N+1)^2 \times 1}$ is a realisation of the circularly invariant complex Gaussian distribution $\mathbf{h} \sim \mathcal{N}_{\mathbb{C}}(\mathbf{0}, \frac{c}{D^2} \mathbf{A} \mathbf{R})$, where \tilde{D} is the average distance between transmitter and receiver [44]. A is the area of a transmit antenna and the entries of the spatial correlation matrix $\mathbf{R} \in \mathbb{C}^{(N+1)^2 \times (N+1)^2}$ are given by

$$R_{ij} = \text{sinc}\left(\frac{2}{\lambda} \sqrt{(a_{xi} - a_{xj})^2 + (a_{zi} - a_{zj})^2}\right), \quad \forall i, j = 1, \dots, (N+1)^2, \quad (24)$$

with $\text{sinc}(x) = \sin(\pi x)/(\pi x)$ [44]. The propagation environment is no longer deterministic in case of small-scale fading. For the simulations, the coefficient of variation (CoV) is provided to indicate the variability of the simulation values in relation to the mean. This dimensionless measure is comparable across the simulation results of different environments. For the simulations, we consider $\kappa = 10$, and $A = (\lambda/2)^2$.

1) Discreteness of the Optimal Solution

We investigate the sparsity of the transmit antenna deployment at LoD $N + 1 = 81$ by calculating the number

of antennas relative to the number of available grid cells $(N + 1)^2$. The optimal distribution of transmit power for an individual channel realisation is determined by solving (22), whereby we utilise the squared magnitude of the Rician channel (23), after normalisation by the reference channel gain c , instead of the normalised squared magnitude of the LoS channel, i.e., $f_{xz}(a_{xi}, a_{zi})$, in the constraints (22b). This yields the optimal number of transmit antennas for an individual channel realisation. Subsequently, we average the optimal number of transmit antennas over the different channel realisations. The results are given in Table 2 and we list the percentage of non-zeros of the proposed deployment developed under LoS conditions for comparison. Table 2

TABLE 2. Average number of transmit antennas relative to number of grid cells under fading conditions compared with the percentage of non-zeros in the proposed distribution developed under LoS conditions at LoD $N + 1 = 81$.

Height Width	LoS [%]	Rician Mean [%]	Rician CoV [%]
1/1	0.152	0.155	77.10
1/3	0.183	0.65	16.81
1/4	0.198	1.14	10.87
1/5	0.61	1.751	10.45

reveals that the distribution of power, when optimised under fading conditions, is less sparse across all environments compared to the distribution of power under perfect LoS conditions, i.e., a larger number of transmit antennas is required. Moreover, the CoV is similar across different environments, except for the environment with a height-to-width ratio of one. This system is especially sensitive to channel fluctuations since under LoS conditions, the optimal deployment requires only a single transmit antenna.

2) Performance Comparison

Next, the performance of the proposed optimal deployment and power allocation is investigated in the small-scale fading environment. For each channel realisation, we determine the minimum received power which is achieved when utilising the proposed deployment and power allocation, which was optimised for LoS conditions. As a benchmark, we optimise the deployment and power allocation for each channel realisation and then determine the received power at the critical receiver positions. We average the minimum received power of the optimal LoS solution and the benchmark scheme across the channel realisations, respectively. The loss in performance due to small-scale fading is measured by the ratio of the averaged objective value of the proposed scheme developed under LoS conditions divided by the averaged objective value of the benchmark scheme. Simulations are performed for environments with different height-to-width ratios and the results are displayed in Table 3.

TABLE 3. Performance loss due to small-scale fading.

Height Width	Average Relative Performance [%]	CoV [%]
1/1	98.752	0.529
1/3	98.77	0.153
1/4	98.79	0.126
1/5	98.8	0.131

The performance loss caused by small-scale fading was found to be below 2% for all considered environments.

VI. CONCLUSION

In this paper, we formulated an optimisation problem for determining the optimal distribution of transmit power across a continuous aperture antenna. The proposed solution maximises the received powers at the worst possible receiver positions in an indoor space. This system is especially relevant for environments with a multitude of mobile low-power devices, which require a reliable supply of power, such as wearables. In this scenario, focusing energy beams to every mobile device may not be possible in a reliable manner. Mathematically, the formulated problem bears a resemblance to that of finding the optimal amplitude-constrained input distribution for achieving the information capacity. Consequently, analogous theoretical results are obtained, which guarantee that the optimal transmit antenna positions are spread out within their area of deployment such that they do not form any regions of concentration and do not occupy any measurable area. Specifically, a transmit antenna architecture with a spatially continuous aperture, which is utilised in HMIMO systems, was proven to be unnecessary for the considered WPT problem. Furthermore, the optimal number of transmit antennas is shown to be finite analytically for a one-dimensional transmit antenna array. Having excluded a continuous aperture antenna as a suitable transmit antenna architecture, the problem was discretised and the resulting solution yielded the optimal transmit antenna deployment including the optimal allocation of transmit power. In the environments investigated through simulation, deploying a finite number of antennas was found to be optimal in all cases. Based on our results, the optimal deployment may be achieved by a finite, and surprisingly small, number of transmit antennas radiating a fixed amount of power. Moreover, our proposed method yields a considerable gain compared to benchmark schemes. Finally, the robustness of the approach has been validated by determining the optimal solution in a fading environment with a strong LoS component. The loss in performance under fading conditions was found to be around 2% in all considered environments.

Possible extensions of the proposed approach offer several opportunities for future work. These include the extension of the method to more geometrically challenging environments and more flexible transmit antenna architecture placements,

such as positioning transmitters on multiple walls as well as the ceiling of a room. Furthermore, a small-scale multipath fading component for modelling the wireless channel may be directly incorporated into the analysis of the problem to improve the robustness of the solution. Moreover, an investigation of the impact of the reactive near-field region when the deployment of large continuous antenna arrays is affordable presents another interesting topic for future work. While we characterise the solution to our problem through tools from topology theory and functional analysis, determining the optimal distribution of power and the transmit antenna deployment through different mathematical techniques may provide additional insights. Furthermore, a possible extension to our problem is the joint optimisation of the amplitudes and the phases of the transmit signals of the individual radiating elements.

Appendix A

By definition, any $P \in \Omega$ is non-negative and bounded by one (see (8)). Observe that given any two distributions $P_1, P_2 \in \Omega$, their convex combination $\lambda P_1 + (1 - \lambda)P_2 \in \Omega$ with coefficient $\lambda \in [0, 1]$ is a distribution as well. It follows that Ω is a convex set [35].

In order to further characterise the set Ω , the weak topology on a Hilbert space is defined. A linear functional in Ω is a linear map from the Hilbert space to the underlying field. The weak topology on a Hilbert space is defined to be the weakest topology such that all continuous linear functionals on the Hilbert space are continuous [47].

Observe that $\mathcal{L}^2(\mathcal{X}_a \times \mathcal{Z}_a)$ is an infinite-dimensional vector space equipped with the following inner product [48]

$$\iint_{\mathcal{X}_a \times \mathcal{Z}_a} w(a_x, a_z) v(a_x, a_z) da_x da_z, \quad \forall w(a_x, a_z), v(a_x, a_z) \in \mathcal{L}^2(\mathcal{X}_a \times \mathcal{Z}_a), \quad (25)$$

where $w(a_x, a_z)$ and $v(a_x, a_z)$ are arbitrary elements of $\mathcal{L}^2(\mathcal{X}_a \times \mathcal{Z}_a)$. This inner product space is complete since completeness is ensured by Lebesgue measurability and Lebesgue integration [48]. Thus, $\mathcal{L}^2(\mathcal{X}_a \times \mathcal{Z}_a)$ is a Hilbert space, which is separable since it has a countable orthonormal basis [48]. Note that the set Ω is a subset of $\mathcal{L}^2(\mathcal{X}_a \times \mathcal{Z}_a)$ with bounded elements in Ω (see (8)). In a separable Hilbert space, every bounded sequence has a weakly convergent subsequence in the weak topology [47] and therefore, Ω is sequentially compact [49]. The concepts of sequential compactness and compactness are equivalent for a separable Hilbert space [47]. Thus, Ω is a compact space.

Appendix B

First, Problem (14) is rewritten in its epigraph form [35] which yields the following constrained optimisation problem

$$\underset{o \in \mathbb{R}, P \in \Omega}{\text{maximise}} \quad o \quad (26a)$$

$$\text{subject to} \quad o \leq \Phi_P\{f_{xz}\}, \quad \forall (x, L_y, z) \in \mathcal{X} \times \mathcal{Y}_{\text{crit}} \times \mathcal{Z}, \quad (26b)$$

where o is bounded by $m = \min_{(x, L_y, z) \in \mathcal{X} \times \mathcal{Y}_{\text{crit}} \times \mathcal{Z}} \Phi_{P^*}\{f_{xz}\}$. Observe

that the objective function and the feasible set of Problem (26) are both affine. Then, if the linear programming problem in (26) admits a solution, i.e., if $o^* = m$ is finite, duality holds. Furthermore, there exist some $\lambda_{xz} \geq 0, \forall (x, L_y, z) \in \mathcal{X} \times \mathcal{Y}_{\text{crit}} \times \mathcal{Z}$ such that the augmented problem

$$\underset{o \in \mathbb{R}, P \in \Omega, \Lambda}{\text{maximise}} \quad o - \sum_{\mathcal{X} \times \mathcal{Y}_{\text{crit}} \times \mathcal{Z}} (o - \Phi_P\{f_{xz}\}) \lambda_{xz}, \quad (27)$$

and Problem (26) are equivalent if the solution (o^*, P^*) is feasible, i.e., the problem constraints are satisfied in (o^*, P^*) , and the following complementary slackness conditions hold:

$$\lambda_{xz} (m - \Phi_{P^*}\{f_{xz}\}) \stackrel{!}{=} 0, \quad \forall (x, L_y, z) \in \mathcal{X} \times \mathcal{Y}_{\text{crit}} \times \mathcal{Z}. \quad (28)$$

Since f_{xz} is bounded, the optimal objective value $o^* = m$ is finite and it is attained in P^* . The conditions in (28) imply

$$\begin{aligned} &[(\lambda_{xz} > 0 \implies m = \Phi_{P^*}\{f_{xz}\}) \text{ or} \\ &(m < \Phi_{P^*}\{f_{xz}\} \implies \lambda_{xz} = 0)], \\ &\forall (x, L_y, z) \in \mathcal{X} \times \mathcal{Y}_{\text{crit}} \times \mathcal{Z} \end{aligned} \quad (29)$$

From (29), if $\lambda_{xz} > 0$, then $o^* = m = \Phi_{P^*}\{f_{xz}\}$ and position (x, L_y, z) is critical. If $o^* = m < \Phi_{P^*}\{f_{xz}\}$, then $\lambda_{xz} = 0$ and position (x, L_y, z) is non-critical. Thus, the dual variables λ_{xz} are only non-zero for critical receiver locations and it is sufficient to sum over $\mathcal{R}_{\text{crit}}$ in (27). Thus, under the assumption that $\mathcal{R}_{\text{crit}}$ is known, the modified augmented problem in (16) along with (29) is equivalent to the augmented problem in (27) together with (29) and thus, to Problem (14).

Appendix C

The continuity of $\Phi_P\{f_{xz}\}$ in P is established in the following lemma.

Lemma C.1. $\Phi_P\{f_{xz}\}$ is weakly continuous in the weak topology on a Hilbert space if f_{xz} is a continuous and bounded function.

Proof:

Based on Theorem 1 in [33], the linear functional $\Phi_P\{f_{xz}\}$ is weakly continuous on Ω if f_{xz} is a continuous and bounded function. From Key Observation 1, f_{xz} is a continuous function and bounded since $y = L_y$. ■

Recall the mathematical equivalence between the WPT problem considered in this paper, where we optimise the transmit power distribution across a continuous aperture antenna and the problem of determining the amplitude-constrained capacity-achieving input distribution of a channel studied in, e.g., [31]–[33]. For the proof of Proposition 1 we apply Theorem 9 in [33]. The convexity and compactness of Ω is established in Lemma 1. The continuity of $J(P)$ is shown in Lemma C.1. The concavity of $J(P)$ follows from the linearity of $J(P)$ in P . Formulating the optimality

condition for P^* requires defining the Gâteaux derivative of $J(P)$.

Definition C.1. The Gâteaux derivative of the function $J : \Omega \rightarrow \mathbb{R}$ at P in the direction of Q with $P, Q \in \Omega$ is defined as follows [33]

$$\Delta_Q J(P) = \lim_{\theta \rightarrow 0} \frac{J((1-\theta)P + \theta Q) - J(P)}{\theta}. \quad (30)$$

Moreover, the Gâteaux derivative of $J(P)$ in (30) can be expressed as [33]

$$\Delta_Q J(P) = J(Q) - J(P), \quad (31)$$

since it is a linear functional of P . Theorem 9 in [33] establishes that if Ω is a convex set and $J(P)$ is continuous, concave, and Gâteaux differentiable, then $J(P)$ attains the maximum value at $P^* \in \Omega$ if and only if $\Delta_P J(P^*) \leq 0, \forall P \in \Omega$. Applying (31) and cancelling the terms that are independent of the distributions P and P^* , we obtain

$$\Delta_P J(P^*) = \sum_{\mathcal{R}^{\text{crit}}} \lambda_{xz} \Phi_P \{f_{xz}\} - \sum_{\mathcal{R}^{\text{crit}}} \lambda_{xz} \Phi_{P^*} \{f_{xz}\}. \quad (32)$$

We can further enforce in (32) the constraints on λ_{xz} and $\Phi_P \{f_{xz}\}$ for the optimal solution P^* in (17). Then, λ_{xz} is only non-zero for critical receiver locations w.r.t. the optimal distribution P^* . Furthermore, the objective value for the critical receiver positions is the constant $\Phi_{P^*} \{f_{xz}\} = m$. By expanding the expectation operator in (32), the optimality condition $\Delta_P J(P^*) \leq 0$ can be expressed as

$$\begin{aligned} & \iint_{\mathcal{X}_a \times \mathcal{Z}_a} \frac{\sum_{\mathcal{R}^{\text{crit}}} f_{xz}(a_x, a_z) \lambda_{xz}}{\sum_{\mathcal{R}^{\text{crit}}} \lambda_{xz}} dP(a_x, a_z) \\ &= \iint_{\mathcal{X}_a \times \mathcal{Z}_a} \bar{f}(a_x, a_z) dP(a_x, a_z) \leq m, \end{aligned} \quad (33)$$

which is satisfied with equality for the optimal distribution of power P^* .

Appendix D

If the conditions (20) and (21) are satisfied, then conditions (18) and (19) in Proposition 1 are satisfied. In the following, we show that the converse holds as well, i.e., if Proposition 1 holds, then Corollary 1 holds as well. We proceed by contradiction and assume that Proposition 1 holds, however, (20) does not hold. In this case, $\exists (a_{x1}, a_{z1}) \in \mathcal{X}_a \times \mathcal{Z}_a$, such that $\bar{f}(a_{x1}, a_{z1}) > m$. Suppose, (a_{x1}, a_{z1}) is the only transmit antenna, i.e., (a_{x1}, a_{z1}) is allocated all the power. Then (18) yields

$$\iint_{\mathcal{X}_a \times \mathcal{Z}_a} \bar{f}(a_x, a_z) dP(a_x, a_z) = \bar{f}(a_{x1}, a_{z1}) > m, \quad (34)$$

which contradicts (18) in Proposition 1. Consequently, if (18) holds, then (20) holds as well.

Next, suppose Proposition 1 holds, however, (21) does not. Define a subset $\mathcal{E}_0(P^*) \subset \mathcal{E}(P^*)$ such that $P^*(\mathcal{E}_0(P^*)) = 0$. Observe that $\bar{f}(a_x, a_z)$ is continuous on \mathbb{R}^2 since the function's numerator is a weighted sum of continuous functions and the denominator is always a positive constant. Assume

there exists a point of increase $(a_{x1}, a_{z1}) \in \mathcal{E}(P^*) \setminus \mathcal{E}_0(P^*)$ such that $\bar{f}(a_{x1}, a_{z1}) > m$. For any $\delta > 0$ such that $\bar{f}(a_{x1}, a_{z1}) - \delta > m$, there exists an open ball \mathcal{B} centred at (a_{x1}, a_{z1}) such that $\bar{f}(a_x, a_z) > \bar{f}(a_{x1}, a_{z1}) - \delta > m, \forall (a_x, a_z) \in \mathcal{B}$, which follows from the continuity of $\bar{f}(a_x, a_z)$. Since the open ball \mathcal{B} contains the point of increase $(a_{x1}, a_{z1}) \in \mathcal{E}(P^*) \setminus \mathcal{E}_0(P^*)$, it follows that $P^*(\mathcal{B}) > 0$. This contradicts Proposition 1, i.e., $m = \iint_{\mathcal{X}_a \times \mathcal{Z}_a} \bar{f}(a_x, a_z) dP^*(a_x, a_z)$, since

$$\begin{aligned} m &= \underbrace{\iint_{(\mathcal{E}(P^*) \setminus \mathcal{E}_0(P^*)) \cap \mathcal{B}} \bar{f}(a_x, a_z) dP^*(a_x, a_z)}_{> mP^*(\mathcal{B})} \\ &+ \underbrace{\iint_{(\mathcal{E}(P^*) \setminus \mathcal{E}_0(P^*)) \setminus \mathcal{B}} \bar{f}(a_x, a_z) dP^*(a_x, a_z)}_{= m(1-P^*(\mathcal{B}))} \\ &+ \underbrace{\iint_{\mathcal{E}_0(P^*)} \bar{f}(a_x, a_z) dP^*(a_x, a_z)}_{=0} > m. \end{aligned} \quad (35)$$

From this contradiction we have shown that $\bar{f}(a_x, a_z) = m, \forall (a_x, a_z) \in \mathcal{E}(P^*) \setminus \mathcal{E}_0(P^*)$. Furthermore, since $P^*(\mathcal{E}_0(P^*)) = 0$, $\mathcal{E}_0(P^*)$ has no interior points. Any open set of \mathbb{R}^2 containing a point in $\mathcal{E}_0(P^*)$ intersects points in $\mathcal{E}(P^*) \setminus \mathcal{E}_0(P^*)$ and therefore, every point in $\mathcal{E}_0(P^*)$ is in the closure of $\mathcal{E}(P^*) \setminus \mathcal{E}_0(P^*)$. Moreover, since $\bar{f}(a_x, a_z)$ is continuous and bounded, it must also be constant on the closure of $\mathcal{E}(P^*) \setminus \mathcal{E}_0(P^*)$. This implies $\bar{f}(a_x, a_z) = m, \forall (a_x, a_z) \in \mathcal{E}(P^*)$. Consequently, if (18) holds, then (21) holds as well. Thus, (20) and (21) are necessary and sufficient conditions for $P^*(a_x, a_z)$.

Appendix E

The proof is similar to Theorem 12 in [33].

The characterisation of the support \mathcal{E} requires the Identity Theorem for real-analytic functions, which is stated, e.g., in [50]. The Identity Theorem states that if two real-analytic functions f_1 and f_2 , which are defined on an open set $U \subseteq \mathbb{R}^n$, take the same value on an open subset $W \subseteq U$, i.e., $f_1(w) = f_2(w), \forall w \in W$, then $f_1(u) = f_2(u), \forall u \in U$.

Next, we show that $\bar{f}(a_x, a_z)$ is not constant in $\mathcal{X}_a \times \mathcal{Z}_a$. Thereby, it suffices to show that the partial derivative of $\bar{f}(a_x, a_z)$ w.r.t. a_x , with $a_z = 0$, is not zero $\forall (a_x, a_z) \in \mathcal{X}_a \times \mathcal{Z}_a$. Note that

$$\frac{\partial \bar{f}(a_x, a_z)}{\partial a_x} = \frac{\sum_{\mathcal{R}^{\text{crit}}} \frac{2(x - a_x)}{\left((z - a_z)^2 + (x - a_x)^2 + L_y^2\right)^2} \lambda_{xz}}{\sum_{\mathcal{R}^{\text{crit}}} \lambda_{xz}}, \quad (36)$$

is only zero for $x = a_x$ and non-zero otherwise. Consequently, $\bar{f}(a_x, a_z)$ is not constant in $\mathcal{X}_a \times \mathcal{Z}_a$.

Next, we show that $\bar{f}(a_x, a_z)$ is real-analytic in \mathbb{R}^2 and thus, in $\mathcal{X}_a \times \mathcal{Z}_a$. Let $\bar{f}(a_x, a_z) = kn(a_x, a_z)$, where $k = \left(\sum_{\mathcal{R}^{\text{crit}}} \lambda_{xz}\right)^{-1}$ is a positive constant for all (a_x, a_z) and

$n(a_x, a_z) = \sum_{\mathcal{R}_{\text{crit}}} f_{xz}(a_x, a_z) \lambda_{xz}$. The function $\bar{f}(a_x, a_z)$ is real-analytic in (a_x, a_z) if $n(a_x, a_z)$ is an analytic function. The function $n(a_x, a_z)$ is real-analytic in (a_x, a_z) if $f_{xz}(a_x, a_z) \lambda_{xz}$ is real-analytic for fixed (x, z) . Thereby, it suffices to show that $f_{xz}(a_x, a_z)$ is real-analytic since λ_{xz} is some non-negative constant scaling $f_{xz}(a_x, a_z)$.

Note that the composition of real-analytic functions is real-analytic [50]. By rewriting $f_{xz}(a_x, a_z)$ as $f(w_{xz}(a_x, a_z)) = 1/(L_y^2 + w_{xz}(a_x, a_z))$, where $w_{xz}(a_x, a_z) = (x - a_x)^2 + (z - a_z)^2 \geq 0$, it is sufficient to show that both $w_{xz}(a_x, a_z)$ and $f(w) = 1/(w + L_y^2) > 0$ are real-analytic. By definition, polynomials are real-analytic functions [50], thus $w_{xz}(a_x, a_z)$ is real-analytic. Next, the real function $f(w)$ is shown to be analytic by proving that its complex extension $f(r_1 + jr_2) = u(r_1, r_2) + jv(r_1, r_2) = (r_1 + L_y^2)/((r_1 + L_y)^2 + r_2^2) - jr_2/((r_1 + L_y)^2 + r_2^2)$ is holomorphic. Function $f(w)$ is holomorphic and thus, analytic, if it satisfies the Cauchy-Riemann (CR) equations [51]. The CR equations are given by [51]

$$\frac{\partial u(r_1, r_2)}{\partial r_1} = \frac{\partial v(r_1, r_2)}{\partial r_2}, \quad (37)$$

$$\frac{\partial u(r_1, r_2)}{\partial r_2} = -\frac{\partial v(r_1, r_2)}{\partial r_1}, \quad (38)$$

Clearly, the CR equations are satisfied for the complex extension $f(r_1 + jr_2)$ since

$$\frac{\partial u(r_1, r_2)}{\partial r_1} = \frac{\partial v(r_1, r_2)}{\partial r_2} = \frac{r_2^2 - (L_y^2 + r_1)^2}{((L_y^2 + r_1)^2 + r_2^2)^2}, \quad (39)$$

$$\frac{\partial u(r_1, r_2)}{\partial r_2} = -\frac{\partial v(r_1, r_2)}{\partial r_1} = \frac{-2r_2(L_y^2 + r_1)}{((L_y^2 + r_1)^2 + r_2^2)^2}, \quad (40)$$

which proves that the complex extension $f(r_1 + jr_2)$ is analytic. Consequently, $\bar{f}(a_x, a_z)$ is real-analytic in $\forall (a_x, a_z) \in \mathbb{R}^2$ and thus, in $\forall (a_x, a_z) \in \mathcal{X}_a \times \mathcal{Z}_a$.

Suppose that $\mathcal{E}(P^*)$ is not a nowhere dense set in $\mathcal{X}_a \times \mathcal{Z}_a$. Consequently, there exists some non-empty open set $\mathcal{E}_2 \subset \mathcal{X}_a \times \mathcal{Z}_a$ such that $\mathcal{E}_2 \cap \mathcal{E}(P^*)$ is dense in $\mathcal{X}_a \times \mathcal{Z}_a$. From (21), $\bar{f}(a_x, a_z) = m$ is constant on $\mathcal{E}(P^*)$ and thus, constant on $\mathcal{E}_2 \cap \mathcal{E}(P^*)$. Since $\bar{f}(a_x, a_z)$ is real-analytic, the Identity Theorem of real-analytic functions applies and thus, $\bar{f}(a_x, a_z)$ must be constant on $\mathcal{X}_a \times \mathcal{Z}_a$. However, $\bar{f}(a_x, a_z) \neq \text{const.}, \forall (a_x, a_z) \in \mathcal{X}_a \times \mathcal{Z}_a$. From this contradiction, $\mathcal{E}(P^*) \subset \mathcal{X}_a \times \mathcal{Z}_a$ must be a nowhere dense set of $\mathcal{X}_a \times \mathcal{Z}_a$.

Appendix F

Suppose $\mathcal{E}(P^*)$ is of positive Lebesgue measure. For any open subset $\mathcal{V} \subset \mathcal{E}(P^*)$, the function $\bar{f}(a_x, a_z)$ is constant on \mathcal{V} since it is constant on $\mathcal{E}(P^*)$. Since $\bar{f}(a_x, a_z)$ is real-analytic as shown in Appendix E, the Identity Theorem, e.g., [50] of real-analytic functions applies and thus, $\bar{f}(a_x, a_z)$ must be constant on $\mathcal{X}_a \times \mathcal{Z}_a$. However, as shown in Appendix E, $\bar{f}(a_x, a_z) \neq \text{const.}, \forall (a_x, a_z) \in \mathcal{X}_a \times \mathcal{Z}_a$. From this contradiction, $\mathcal{E}(P^*) \subset \mathcal{X}_a \times \mathcal{Z}_a$ must have Lebesgue measure zero.

Appendix G

The proof is also analogous to [31], [32].

This proof requires the application of the Bolzano-Weierstrass theorem which states that in the set of real numbers any infinite bounded sequence of real numbers has a convergent subsequence and the limit of that subsequence is an accumulation point of the original sequence [52]. In the following $\bar{f}(a_l)$ is a function defined over a one-dimensional set, i.e., $f: \mathcal{L}_a \rightarrow \mathbb{R}$, with $\mathcal{L}_a \subset \mathcal{X}_a \times \mathcal{Z}_a$ and $\tilde{\mathcal{E}}(\tilde{P}^*)$ is the optimal set of transmit antenna positions, which is bounded, i.e., $\tilde{\mathcal{E}}(\tilde{P}^*) \subset \mathcal{L}_a$. Suppose the set $\tilde{\mathcal{E}}(\tilde{P}^*)$ is not finite. From the Bolzano-Weierstrass theorem, it follows that $\tilde{\mathcal{E}}(\tilde{P}^*)$ has an accumulation point q . Based on (21), define the function $s(a_l) = m - \bar{f}(a_l)$, which is equal to zero $\forall a_l \in \tilde{\mathcal{E}}$. Moreover, $s(a_l)$ is analytic since it is the sum of analytic functions [50]. By assuming $\tilde{\mathcal{E}}(\tilde{P}^*)$ is not finite, s has infinitely many zeros. Moreover, the accumulation point q is also a zero of function $s(a_l)$, i.e., $s(q) = 0$, since $s(a_l)$ is a continuous function, which is implied by the analyticity of $s(a_l)$. Then, from the Identity Theorem, e.g. [50], $s(a_l)$ coincides with zero in the entire set \mathcal{L}_a or equivalently

$$\bar{f}(a_l) = m, \forall a_l \in \mathcal{L}_a, \quad (41)$$

which implies that \bar{f} is constant on \mathcal{L}_a . However, \bar{f} is not constant on \mathcal{L}_a as shown in Appendix E. Consequently, $\tilde{\mathcal{E}}(\tilde{P}^*)$ must be a finite set.

REFERENCES

- [1] H. Rahmani, D. Shetty, M. Wagih, et al., "Next-generation IoT devices: Sustainable eco-friendly manufacturing, energy harvesting, and wireless connectivity," *IEEE J. Microwaves*, vol. 3, pp. 237–255, Jan. 2023.
- [2] F. John Dian, R. Vahidnia, and A. Rahmati, "Wearables and the internet of things (IoT), applications, opportunities, and challenges: A survey," *IEEE Access*, vol. 8, pp. 69200–69211, Apr. 2020.
- [3] D. Verma, K. R. Singh, A. K. Yadav, et al., "Internet of things (IoT) in nano-integrated wearable biosensor devices for healthcare applications," *Biosens. Bioelectron.*: X, vol. 11, Sep. 2022.
- [4] D. Metcalf, S. T. Milliard, M. Gomez, and M. Schwartz, "Wearables and the internet of things for health: Wearable, interconnected devices promise more efficient and comprehensive health care," *IEEE Pulse*, vol. 7, pp. 35–39, Sept.-Oct. 2016.
- [5] M. Wagih, L. Balocchi, F. Benassi, et al., "Microwave-enabled wearables: Underpinning technologies, integration platforms, and next-generation roadmap," *IEEE J. Microwaves*, vol. 3, pp. 193–226, Jan. 2023.
- [6] M. Wagih, A. S. Weddell, and S. Beeby, "Millimeter-wave power harvesting: A review," *IEEE Open J. Antennas Propag.*, vol. 1, pp. 560–578, Dec. 2020.
- [7] O. L. A. López, D. Kumar, R. D. Souza, P. Popovski, A. Tölli, and M. Latva-Aho, "Massive MIMO with radio stripes for indoor wireless energy transfer," *IEEE Trans. Wirel. Commun.*, vol. 21, pp. 7088–7104, Sep. 2022.
- [8] O. López, S. Montejo-Sánchez, R. D. Souza, C. B. Papadias, and H. Alves, "On CSI-free multiantenna schemes for massive RF wireless energy transfer," *IEEE Internet Things J.*, vol. 8, pp. 278–296, Jan. 2021.
- [9] O. López, H. Alves, R. D. Souza, S. Montejo-Sánchez, E. M. G. Fernández, and M. Latva-Aho, "Massive wireless energy transfer: Enabling sustainable IoT toward 6G era," *IEEE Internet Things J.*, vol. 8, pp. 8816–8835, Jun 2021.
- [10] Z. Wang, J. Zhang, H. Du, D. Niyato, S. Cui, B. Ai, M. Debbah, K. B. Letaief, and H. V. Poor, "A tutorial on extremely large-scale MIMO for 6G: Fundamentals, signal processing, and applications," *IEEE Commun. Surv. Tutor.*, pp. 1–1, Jan. 2024.

- [11] E. Björnson, L. Sanguinetti, H. Wymeersch, J. Hoydis, and T. L. Marzetta, “Massive MIMO is a reality—what is next?: Five promising research directions for antenna arrays,” *Digit. Signal Process.*, vol. 94, pp. 3–20, Feb. 2019.
- [12] C. Huang, S. Hu, G. C. Alexandropoulos, *et al.*, “Holographic MIMO surfaces for 6G wireless networks: Opportunities, challenges, and trends,” *IEEE Wirel. Commun.*, vol. 27, pp. 118–125, Oct. 2020.
- [13] K. Anusuya, S. Bharadhwaj, and S. Subha Rani, “Wireless channel models for indoor environments,” *Defence Science Journal*, vol. 58, 11 2008.
- [14] M. M. Abdulwahid, O. A. S. Al-Ani, M. F. Mosleh, and R. A. Abd-Alhameed, “A comparison between different C-band and mmWave band frequencies for indoor communication,” *J. Commun.*, vol. 14, no. 10, pp. 892–899, 2019.
- [15] P. Liu, M. Di Renzo, and A. Springer, “Line-of-sight spatial modulation for indoor mmWave communication at 60 GHz,” *IEEE Trans. Wirel. Commun.*, vol. 15, no. 11, pp. 7373–7389, 2016.
- [16] N. S. Perović, M. D. Renzo, and M. F. Flanagan, “Channel capacity optimization using reconfigurable intelligent surfaces in indoor mmWave environments,” in *Proc. IEEE Int. Conf. Commun.*, pp. 1–7, 2020.
- [17] H. Zhang, N. Shlezinger, F. Guidi, D. Dardari, M. F. Imani, and Y. C. Eldar, “Near-field wireless power transfer for 6G internet of everything mobile networks: Opportunities and challenges,” *IEEE Commun. Mag.*, vol. 60, pp. 12–18, Mar. 2022.
- [18] H. Zhang, N. Shlezinger, F. Guidi, D. Dardari, and Y. C. Eldar, “6G wireless communications: From far-field beam steering to near-field beam focusing,” *IEEE Commun. Mag.*, vol. 61, pp. 72–77, Apr. 2023.
- [19] S. Hu, F. Rusek, and O. Edfors, “Beyond massive MIMO: The potential of data transmission with large intelligent surfaces,” *IEEE Trans. Signal Process.*, vol. 66, pp. 2746–2758, May 2018.
- [20] D. Dardari and N. Decarli, “Holographic communication using intelligent surfaces,” *IEEE Commun. Mag.*, vol. 59, pp. 35–41, June 2021.
- [21] O. M. Rosabal, O. L. A. López, H. Alves, S. Montejo-Sánchez, and M. Latva-Aho, “On the optimal deployment of power beacons for massive wireless energy transfer,” *IEEE Internet Things J.*, vol. 8, pp. 10531–10542, Jul. 2021.
- [22] X. Jia and X. Zhou, “Power beacon placement for maximizing guaranteed coverage in bistatic backscatter networks,” *IEEE Trans. Commun.*, vol. 69, pp. 7895–7909, Nov. 2021.
- [23] S. Zhou, H. Dai, H. Sun, G. Tan, and B. Ye, “On the deployment of clustered power beacons in random wireless powered communication,” *IEEE Trans. Veh.*, vol. 72, pp. 2424–2438, Feb. 2023.
- [24] H. Tabassum and E. Hossain, “On the deployment of energy sources in wireless-powered cellular networks,” *IEEE Trans. Commun.*, vol. 63, pp. 3391–3404, Sep. 2015.
- [25] A. Azarbahram, O. López, P. Popovski, and M. Latva-Aho, “On the radio stripe deployment for indoor RF wireless power transfer,” *arXiv preprint arXiv:2310.09585*, 2023.
- [26] E. Björnson and L. Sanguinetti, “Power scaling laws and near-field behaviors of massive MIMO and intelligent reflecting surfaces,” *IEEE Open J. Commun. Soc.*, vol. 1, pp. 1306–1324, 2020.
- [27] Y. Liu, Z. Wang, J. Xu, C. Ouyang, X. Mu, and R. Schober, “Near-field communications: A tutorial review,” *IEEE Open J. Commun. Soc.*, vol. 4, pp. 1999–2049, 2023.
- [28] H. Do, S. Cho, J. Park, H.-J. Song, N. Lee, and A. Lozano, “Terahertz line-of-sight MIMO communication: Theory and practical challenges,” *IEEE Commun. Mag.*, vol. 59, pp. 104–109, Mar. 2021.
- [29] X. Li, H. Lu, Y. Zeng, S. Jin, and R. Zhang, “Near-field modelling and performance analysis of modular extremely large-scale array communications,” *IEEE Commun. Lett.*, vol. 26, pp. 1529–1533, Jul. 2022.
- [30] H. Zhang, N. Shlezinger, F. Guidi, D. Dardari, M. F. Imani, and Y. C. Eldar, “Beam focusing for near-field multiuser MIMO communications,” *IEEE Trans. Wirel. Commun.*, vol. 21, pp. 7476–7490, Sep. 2022.
- [31] J. G. Smith, “The information capacity of amplitude- and variance-constrained scalar Gaussian channels,” *Inf. Control.*, vol. 18, pp. 203–219, Apr. 1971.
- [32] R. Morsi, V. Jamali, A. Hagelauer, D. W. K. Ng, and R. Schober, “Conditional capacity and transmit signal design for SWIPT systems with multiple nonlinear energy harvesting receivers,” *IEEE Trans. Commun.*, vol. 68, pp. 582–601, Jan. 2020.
- [33] A. Dytso, M. Goldenbaum, H. V. Poor, and S. S. Shitz, “When are discrete channel inputs optimal? — Optimization techniques and some new results,” in *Proc. 52nd Annu. Conf. Inf. Sci. Syst.*, pp. 1–6, 2018.
- [34] B. Clerckx, J. Kim, K. W. Choi, and D. I. Kim, “Foundations of wireless information and power transfer: Theory, prototypes, and experiments,” *Proc. IEEE*, vol. 110, pp. 8–30, Jan. 2022.
- [35] S. P. Boyd and L. Vandenberghe, *Convex Optimization*. Cambridge, UK: Cambridge University Press, 2004.
- [36] S. Diamond and S. Boyd, “CVXPY: A python-embedded modeling language for convex optimization,” *J. Mach. Learn. Res.*, vol. 17, pp. 1–5, Mar. 2016.
- [37] A. Agrawal, R. Verschueren, S. Diamond, and S. Boyd, “A rewriting system for convex optimization problems,” *J. Control Decis.*, vol. 5, pp. 42–60, Jan. 2018.
- [38] A. Collado and A. T. Georgiadis, “24 GHz substrate integrated waveguide (SIW) rectenna for energy harvesting and wireless power transmission,” *2013 IEEE MTT-S International Microwave Symposium Digest (MTT)*, pp. 1–3, 2013.
- [39] M. K. L. Alhasnawi, S. Abdulla, D. Fatseas, and R. G. Addie, “Spectral density constraints on wireless communication,” *Heliyon*, vol. 6, May 2020.
- [40] Y. Liu, J. Xu, Z. Wang, X. Mu, and L. Hanzo, “Near-field communications: What will be different?,” *arXiv preprint arXiv:2303.04003*, 2023.
- [41] B. Clerckx, R. Zhang, R. Schober, D. W. K. Ng, D. I. Kim, and H. V. Poor, “Fundamentals of wireless information and power transfer: From RF energy harvester models to signal and system designs,” *IEEE J. Sel. Areas Commun.*, vol. 37, pp. 4–33, Jan. 2019.
- [42] R. H. Olsson, C. Gordon, and R. Bogoslovov, “Zero and near zero power intelligent microsystems,” *J. Phys.: Conf. Ser.*, vol. 1407, Nov. 2019.
- [43] D. Tse and P. Viswanath, *Fundamentals of Wireless Communication*. Cambridge, UK: Cambridge University Press, 2005.
- [44] E. Björnson and L. Sanguinetti, “Rayleigh fading modeling and channel hardening for reconfigurable intelligent surfaces,” *IEEE Wirel. Commun. Lett.*, vol. 10, pp. 830–834, Apr. 2021.
- [45] A. Pizzo, T. L. Marzetta, and L. Sanguinetti, “Spatially-stationary model for holographic MIMO small-scale fading,” *IEEE J. Sel. Areas Commun.*, vol. 38, pp. 1964–1979, Sept. 2020.
- [46] E. Björnson, J. Hoydis, and L. Sanguinetti, “Massive MIMO networks: Spectral, energy, and hardware efficiency,” *Found. Trends Signal Process.*, vol. 11, no. 3-4, pp. 154–655, 2017.
- [47] W. Rudin, *Functional Analysis*. McGraw Hill, 1991.
- [48] M. Vetterli, J. Kovačević, and V. K. Goyal, *Foundations of Signal Processing*. Cambridge, UK: Cambridge University Press, 2014.
- [49] S. Willard, *General Topology*. Dover Publications, 2004.
- [50] S. G. Krantz and H. R. Parks, *A Primer of Real Analytic Functions*. Springer, 2002.
- [51] W. Rudin, *Real and Complex Analysis*. McGraw Hill, 1987.
- [52] W. Rudin, *Principles of Mathematical Analysis*. McGraw Hill, 1976.



KENNETH M. MAYER (Graduate Student Member, IEEE) received the B.Sc. degree in Medical Engineering (2019) and the M.Sc. degree in Advanced Signal Processing and Communications Engineering (2021) from Friedrich-Alexander University (FAU) Erlangen-Nuremberg, Germany. He is currently pursuing the Ph.D. degree at the Institute for Digital Communications at FAU focusing on wireless communications and wireless power transfer.



LAURA COTTATELLUCCI (Member, IEEE) received the M.Sc. degree in electrical engineering from La Sapienza University of Rome, Italy, the Ph.D. degree from Technical University of Vienna, Austria (2006), and the Habilitation degree from University of Nice-Sophia Antipolis, France. Since December 2017 and September 2021, she has been a professor for digital communications at Friedrich Alexander Universität (FAU) Erlangen-Nuremberg, Germany, and an Adjunct Professor at EURECOM, France, respectively. She worked for

5 years (1995-2000) at Telecom Italia in the design of telecommunications networks and as Senior Researcher at Forschungszentrum Telekommunikation Wien, Austria (2000-2005). She was a Research Fellow at INRIA, France, in the quarter October-December 2005, and at the University of South Australia in 2006. From December 2006 to November 2017, she was an Assistant Professor at EURECOM, France, where she was also an Adjunct Professor (2018-2019). She was an Elected Member of the IEEE Technical Committee on Signal Processing for Communications and Networking (2017-22), served as an Associate Editor for the IEEE TRANSACTIONS ON COMMUNICATIONS (2015-2020) and the IEEE TRANSACTIONS ON SIGNAL PROCESSING (2016- 2020). Since September 2022 she has been senior member of the editorial board of IEEE *Signal Processing Magazine*. Her research interests are in the field of communication and information theory and signal processing for wireless communications, satellite, and complex networks.



ROBERT SCHOBER (Fellow, IEEE) received the Diplom (Univ.) and the Ph.D. degrees in electrical engineering from Friedrich-Alexander University of Erlangen-Nuremberg (FAU), Germany, in 1997 and 2000, respectively. From 2002 to 2011, he was a Professor and Canada Research Chair at the University of British Columbia (UBC), Vancouver, Canada. Since January 2012 he is an Alexander von Humboldt Professor and the Chair for Digital Communication at FAU. His research interests fall into the broad areas of Communication Theory, Wireless and Molecular Communications, and Statistical Signal Processing.

tion Theory, Wireless and Molecular Communications, and Statistical Signal Processing.

Robert received several awards for his work including the 2002 Heinz Maier Leibnitz Award of the German Science Foundation (DFG), the 2004 Innovations Award of the Vodafone Foundation for Research in Mobile Communications, a 2006 UBC Killam Research Prize, a 2007 Wilhelm Friedrich Bessel Research Award of the Alexander von Humboldt Foundation, the 2008 Charles McDowell Award for Excellence in Research from UBC, a 2011 Alexander von Humboldt Professorship, a 2012 NSERC E.W.R. Stacie Fellowship, a 2017 Wireless Communications Recognition Award by the IEEE Wireless Communications Technical Committee, and the 2022 IEEE Vehicular Technology Society Stuart F. Meyer Memorial Award. Furthermore, he received numerous Best Paper Awards for his work including the 2022 ComSoc Stephen O. Rice Prize and the 2023 ComSoc Leonard G. Abraham Prize. Since 2017, he has been listed as a Highly Cited Researcher by the Web of Science. Robert is a Fellow of the Canadian Academy of Engineering, a Fellow of the Engineering Institute of Canada, and a Member of the German National Academy of Science and Engineering.

He served as Editor-in-Chief of the IEEE TRANSACTIONS ON COMMUNICATIONS, VP Publications of the IEEE Communication Society (ComSoc), ComSoc Member at Large, and ComSoc Treasurer. Currently, he serves as Senior Editor of the PROCEEDINGS OF THE IEEE and as ComSoc President.